ANNUAL REVIEWS

Annual Review of Fluid Mechanics

Numerical Methods for Viscoelastic Fluid Flows

M.A. Alves,[1] P.J. Oliveira,[2] and F.T. Pinho[3]

[1]CEFT (Centro de Estudos de Fenómenos de Transporte), Departamento de Engenharia Química, Faculdade de Engenharia, Universidade do Porto, 4200-465 Porto, Portugal; email: mmalves@fe.up.pt

[2]C-MAST (Center for Mechanical and Aerospace Science and Technologies), Departamento de Engenharia Electromecânica, Faculdade de Engenharia, Universidade da Beira Interior, 6201-001 Covilhã, Portugal; email: pjpo@ubi.pt

[3]CEFT, Departamento de Engenharia Mecânica, Faculdade de Engenharia, Universidade do Porto, 4200-465 Porto, Portugal; email: fpinho@fe.up.pt

Annu. Rev. Fluid Mech. 2021. 53:509–41

First published as a Review in Advance on November 3, 2020

The *Annual Review of Fluid Mechanics* is online at fluid.annualreviews.org

https://doi.org/10.1146/annurev-fluid-010719-060107

Keywords

computational rheology, finite-volume method, viscoelastic flows, high–Weissenberg number problem, benchmark flows, numerical stabilization methods

Abstract

Complex fluids exist in nature and are continually engineered for specific applications involving the addition of macromolecules to a solvent, among other means. This imparts viscoelasticity to the fluid, a property responsible for various flow instabilities and major modifications to the fluid dynamics. Recent developments in the numerical methods for the simulation of viscoelastic fluid flows, described by continuum-level differential constitutive equations, are surveyed, with a particular emphasis on the finite-volume method. This method is briefly described, and the main benchmark flows currently used in computational rheology to assess the performance of numerical methods are presented. Outstanding issues in numerical methods and novel and challenging applications of viscoelastic fluids, some of which require further developments in numerical methods, are discussed.

1. INTRODUCTION

Many synthetic fluids, as well as some natural fluids, show complex rheological behavior in which viscoelasticity is a relevant fluid property. Over the last 40 years, computational rheology (CR), the application of computational fluid dynamics (CFD) to fluids with non-Newtonian rheology, has developed into a mature discipline, which simultaneously helps to understand a wide range of physical phenomena while also providing useful tools for engineering design. CR refers to flow simulations with fluids that are described by non-Newtonian models, more complex than the generalized Newtonian fluid, since specific techniques to address the inherent numerical difficulties associated with the complex constitutive equations are needed even if the simulations are aimed at a fluid mechanics perspective.

In the late 1970s, at a time when Newtonian CFD had already started to materialize into competing commercial products, the large scatter of numerical results for the same viscoelastic non-Newtonian flow problems and the corresponding conflicting physical interpretations of data, which were very much associated with the lack of accuracy and convergence difficulties ensuing from the so-called high–Weissenberg number problem (HWNP), led to the establishment of a series of regular workshops that introduced proper benchmarks and focused research efforts in the field. The biannual International Workshop on Numerical Methods in Non-Newtonian Flows started in 1979 in Rhode Island, USA, and had its nineteenth edition in 2019, in Peso da Régua, Portugal. The beginning of the twenty-first century saw significant progress in tackling the HWNP through a better understanding of its causes and the ensuing development of various appropriate numerical techniques. CR could at last be used in uncharted territory in the Weissenberg number (*Wi*)–Reynolds number (*Re*) phase space, thus becoming a more accurate and trustworthy tool, provided that the adequate constitutive equation is selected for the particular fluid and flow under investigation.

The relevance of this last point should be emphasized. If we take for granted the description of structurally simple fluids as Newtonian, in all possible flows, the description of complex fluids is often incomplete, except for very limited simple flow kinematics. Therefore, numerical or analytical flow descriptions in many real flows will be qualitative at most. In this review, we do not address the difficulties associated with the proper rheological characterization of real fluids by adequate constitutive equations, an important area of research on its own (Bird & Wiest 1995, Larson & Desai 2015); rather, we assume that the adopted model adequately describes the intended fluid properties. Therefore, the numerical methods discussed here are for constitutive equations at the same level of description as the equations governing the conservation of mass and momentum, i.e., at the continuum level, also called macroscopic-scale level. Nevertheless, at the end of this review, we provide some references for methods relying on mesoscopic-scale-level fluid descriptions.

An early textbook, written by Crochet et al. (1984), discussed numerical methods for viscoelastic fluid flows based on the finite-element method (FEM) and finite-difference method (FDM). The enormous progress over the following two decades was covered by Owens & Phillips (2002), but the finite-volume method (FVM) was not addressed in detail. The FVM is a relative latecomer to CR and its extension for viscoelastic fluids has been presented in some detail by Afonso et al. (2012a), but further developments and new computational tools have become available since then. Therefore, this review focuses essentially on the state of the art, leaning toward the FVM, while providing potential future lines of research in numerical methods and new applications in viscoelastic fluid flow simulations.

In the next section, we present the governing equations for viscoelastic fluids in the stress and conformation tensor formulations. The numerical methods used in both approaches are reviewed in Section 3 and related issues in need of investigation are identified. The assessment of the

methods through relevant benchmark flows in CR is the subject of Section 4. At the end of this review, we briefly suggest some topics of future investigation, focusing on applications, as these are the engines of further developments in numerical methods.

2. GOVERNING EQUATIONS

Viscoelastic fluid flows are described by the mass conservation, momentum, and rheological constitutive equations. When temperature variations are important, the energy equation also needs to be included (a topic not covered here) since, from a numerical point of view, it brings no new significant challenge. Although the investigation of some flow instabilities has relied on the assumption of fluid compressibility (Keshtiban et al. 2004), liquid fluids are usually considered incompressible, and this review focuses only on incompressible fluid flows for which the mass conservation simplifies to

$$\nabla \cdot \mathbf{u} = 0. \tag{1.}$$

The momentum equation is

$$\rho \frac{\mathrm{D}\mathbf{u}}{\mathrm{D}t} = -\nabla p + \nabla \cdot \boldsymbol{\tau} + \rho \mathbf{g} \tag{2.}$$

and requires a statement of the fluid rheological behavior via the extra stress tensor ($\boldsymbol{\tau}$), which must be described by an adequate constitutive equation. In these equations ρ is the fluid density, p is the pressure, t is time, $\mathbf{g}$ is the gravitational acceleration, and $\mathbf{u}$ is the velocity vector.

In a basic taxonomic classification, the rheological constitutive equation can be formulated in different ways, and this has numerical implications to be discussed in Section 3. We first consider a stress formulation, where the dependent variable is the extra stress, followed by a conformation formulation, where the conformation tensor ($\mathbf{A}$) is an intermediate structural dependent variable, with the extra stress given through an explicit relation on $\mathbf{A}$.

The earliest viscoelastic models appeared in the context of continuum mechanics, but only after the proper invariant formulations defined by Oldroyd (1950) could they be used to adequately describe flows with large deformations and deformation rates. Such early constitutive equations are the upper-convected Maxwell (UCM), Oldroyd-B, or corotational Maxwell models, to name a few, which are differential-type equations on the extra stress. These are stress formulation models and the early numerical methods were aimed at them. Only some of the constitutive equations allowed by continuum mechanics described real behavior, and the next generation of more sophisticated models was developed based on insights into the structural behavior of complex fluids. The concept of networks of interacting polymer macromolecules was applied to develop continuum-based models for polymer melts and concentrated polymer solutions such as the Phan-Thien–Tanner (PTT) equation (Phan-Thien & Tanner 1977) and the Giesekus equation (Giesekus 1982).

The constitutive equation for the total extra stress tensor $\boldsymbol{\tau}$ can be written in compact form as the sum of a polymer stress $\boldsymbol{\tau}_\mathrm{p}$ with a solvent stress $\boldsymbol{\tau}_\mathrm{s}$,

$$\boldsymbol{\tau} = \boldsymbol{\tau}_\mathrm{p} + \boldsymbol{\tau}_\mathrm{s}, \tag{3.}$$

as required to describe a wide range of fluids from dilute to concentrated polymer solutions and polymer melts for which the solvent stress is negligible. Usually the solvent obeys Newton's law of viscosity,

$$\boldsymbol{\tau}_\mathrm{s} = 2\eta_\mathrm{s}\mathbf{S}, \text{ with } \mathbf{S} = \frac{1}{2}\left(\nabla\mathbf{u} + \nabla\mathbf{u}^\mathrm{T}\right), \tag{4.}$$

where η_s is the solvent shear viscosity (in non-Newtonian fluid mechanics the term "dynamic viscosity" is often used for the ratio between in-phase components of the shear stress and the shear

rate in a small-amplitude oscillatory shear flow) and $\mathbf{S}$ is the rate of strain tensor. The polymer stress is usually described by an integro-differential equation where the stress depends on present and past flow history. This review focuses exclusively on differential constitutive models. For integral constitutive equations, good starting points are the books of Bird et al. (1987a) and Larson (1988). Dealing numerically with integral models relies on Eulerian approaches for some specific flows, but especially on extensions of Lagrangian approaches, as well as on the more recent method of deformation fields. These techniques were reviewed by Keunings (2003) within the scope of FEM, but they can also be used in other frameworks; the method of deformation fields was used in an FDM approach by Tomé et al. (2008).

A general differential equation for $\boldsymbol{\tau}_\mathrm{p}$ containing the UCM model ($\alpha = \varepsilon = \xi = \eta_\mathrm{s} = 0$), the PTT model ($\alpha = 0$), and the Giesekus model ($\varepsilon = \xi = 0$) can be written as

$$Y(\boldsymbol{\tau}_\mathrm{p})\boldsymbol{\tau}_\mathrm{p} + \lambda\left[\overset{\nabla}{\boldsymbol{\tau}}_p + \xi\left(\mathbf{S}\cdot\boldsymbol{\tau}_\mathrm{p} + \boldsymbol{\tau}_\mathrm{p}\cdot\mathbf{S}\right)\right] + \frac{\alpha\lambda}{\eta_\mathrm{p}}\boldsymbol{\tau}_\mathrm{p}\cdot\boldsymbol{\tau}_\mathrm{p} = 2\eta_\mathrm{p}\mathbf{S}, \qquad 5.$$

where $\overset{\nabla}{\boldsymbol{\tau}}_\mathrm{p}$ represents the upper-convected derivative of tensor $\boldsymbol{\tau}_\mathrm{p}$, defined as

$$\overset{\nabla}{\boldsymbol{\tau}}_\mathrm{p} = \frac{\mathrm{D}\boldsymbol{\tau}_\mathrm{p}}{\mathrm{D}t} - \left(\boldsymbol{\tau}_\mathrm{p}\cdot\boldsymbol{\nabla}\mathbf{u} + \boldsymbol{\nabla}\mathbf{u}^\mathrm{T}\cdot\boldsymbol{\tau}_\mathrm{p}\right), \qquad 6.$$

and $Y(\boldsymbol{\tau}_\mathrm{p})$ equals 1 or can be written as

$$Y(\boldsymbol{\tau}_\mathrm{p}) = \exp\left[\frac{\varepsilon\lambda}{\eta_\mathrm{p}}\mathrm{tr}\left(\boldsymbol{\tau}_\mathrm{p}\right)\right] \text{ and } Y\left(\boldsymbol{\tau}_\mathrm{p}\right) = 1 + \frac{\varepsilon\lambda}{\eta_\mathrm{p}}\mathrm{tr}\left(\boldsymbol{\tau}_\mathrm{p}\right) \qquad 7.$$

for the exponential and the linear PTT models, respectively. The relaxation time λ and the zero-shear-rate polymer viscosity η_p are included in all models. To describe the rheology of a specific fluid, one can combine any of these with a solvent stress if necessary. For instance, the Giesekus and PTT models were developed for polymer melts and concentrated polymer solutions (Phan-Thien & Tanner 1977, Giesekus 1982), respectively, for which the solvent viscosity is null or negligible, but generally they can incorporate a solvent contribution.

The Oldroyd-B model results when $\alpha = \varepsilon = \xi = 0$, but it can also be written on the basis of the total extra stress as

$$\boldsymbol{\tau} + \lambda\overset{\nabla}{\boldsymbol{\tau}} = 2\eta_0\left[\mathbf{S} + \lambda_\mathrm{r}\overset{\nabla}{\mathbf{S}}\right], \qquad 8.$$

where $\eta_0 \equiv \eta_\mathrm{s} + \eta_\mathrm{p}$ is the zero-shear-rate viscosity of the solution and $\lambda_\mathrm{r} \equiv \lambda\eta_\mathrm{s}/\eta_0$ is the retardation time. Some models depend on other types, or on combinations, of convected derivatives (Bird et al. 1987a).

Any of these models can be expressed in a multimode version to better describe the rheology of fluids having a spectrum of relaxation times (due to the polydispersity of macromolecules), an idea that has been around for more than a century in the form of the generalized Maxwell model (or Maxwell–Wiechert model) (cf. Bird et al. 1987a). In a multimode model, the polymer stress is given as the sum of N modes,

$$\boldsymbol{\tau}_\mathrm{p} = \sum_{k=1}^{N}\boldsymbol{\tau}_{\mathrm{p},k}, \qquad 9.$$

where the stress from each mode k follows an expression like Equation 5, thus defining spectra of coefficients $(\alpha_k, \varepsilon_k, \lambda_k, \eta_{\mathrm{p},k}, \xi_k)$.

Other rheological equations of differential type that describe different types of polymer melts are the Pom-Pom (McLeish & Larson 1998), XPP [extended Pom-Pom (Verbeeten et al. 2001)], or Rolie-Poly (Likhtman & Graham 2003), to name a few. From a numerical point of view these

models do not introduce new significant challenges; hence, they are not further discussed. Some constitutive models are usually written in the conformation or in a conformation-inspired formulation, in the sense of relying on an intermediate dependent variable of a structural nature other than the conformation tensor, which is discussed next.

Structural models, such as kinetic theory–based models, started to be developed early on. For polymer solutions, the polymer stress is given as a function of a geometric tensor of a mesoscopic description of the structure of the material (some models may depend on more than one descriptor), such as the conformation tensor $\mathbf{A}$ in a dumbbell model. A dumbbell, the simplest of the so-called bead–spring models, is described by two small spheres connected by a spring, with each bead acted upon by solvent viscous forces, the connecting spring force, and Brownian forces. The dumbbell represents ensembles of polymer molecules, and a differential equation describes the evolution of the conformation tensor, where $\mathbf{A} = \langle \mathbf{QQ} \rangle / Q_{\text{eq}}^2$ is the normalized square of the dumbbell end-to-end vector $\mathbf{Q}$ (Q_{eq}^2 is the square of the end-to-end vector magnitude at equilibrium: $Q_{\text{eq}}^2 = \langle \mathbf{Q} \cdot \mathbf{Q} \rangle_{\text{eq}}/3$), so that $\mathbf{A} = \mathbf{I}$ at rest. The dumbbell model is the simplest one representing the main effects of flows on dilute polymer solutions, namely, fluid elasticity, the orientation of the macromolecules relative to the principal axis of strain, and their finite extensibility. It has become known as the finitely extensible nonlinear elastic (FENE) model when the spring force is $\mathbf{F} = H\mathbf{Q}/[1 - (Q/Q_0)^2]$, where Q/Q_0 is the normalized dumbbell extension and H is the spring coefficient. As discussed by Bird et al. (1987b), the ensuing force balance would then need to be solved at the mesoscopic level and its results averaged over many realizations in order to provide the continuum-level polymer stress, but under suitable approximations, like that of Peterlin, the closed form FENE-P macroscopic model is obtained. Variants of the FENE-P model have appeared in the literature, as briefly summarized below.

Even though the FENE-P model was derived on the basis of the conformation tensor $\mathbf{A}$, it was originally presented by Bird et al. (1980) in the stress formalism, in a nonconservative form, as

$$f\left(\boldsymbol{\tau}_{\text{p}}\right)\boldsymbol{\tau}_{\text{p}} + \lambda \overset{\triangledown}{\boldsymbol{\tau}}_{\text{p}} - \left[\lambda \boldsymbol{\tau}_{\text{p}} + a\eta_{\text{p}}\mathbf{I}\right] \frac{\text{D} \ln f\left(\boldsymbol{\tau}_{\text{p}}\right)}{\text{D}t} = 2a\eta_{\text{p}}\mathbf{S}, \qquad 10.$$

where $f(\boldsymbol{\tau}_{\text{p}}) = 1 + 3[1 + \text{tr}\boldsymbol{\tau}_{\text{p}}/3nkT]/b$ is the stress or extensibility function, designated Z in the original paper; $\eta_{\text{p}} = nkT\lambda b/(b+3)$ is the polymer contribution to the viscosity at zero shear rate; λ is the relaxation time; the extensibility function at equilibrium is $f_{\text{eq}} = a \equiv (b+3)/b$; and $b = Q_0^2 H/kT$ is the normalized maximum extensibility. Often one uses instead the parameter $L^2 = Q_0^2/Q_{\text{eq}}^2$, which gives the square of the maximum dumbbell extension relative to its value at equilibrium, and the two are related by $L^2 = b + 3$ in the original FENE-P model.

The FENE-P, in its various forms, and other presented models can be written in closed form using the conformation tensor formalism, which has specific numerical procedures discussed in Section 3. As for the stress formalism above, a general constitutive equation (here for $\xi = 0$) is written in terms of the conformation tensor $\mathbf{A}$ as

$$\boldsymbol{\tau}_{\text{p}} = \frac{\eta_{\text{p}}}{\lambda}\left[f(\mathbf{A})\,\mathbf{A} - g(\mathbf{A})\,\mathbf{I}\right], \qquad 11.$$

with the evolution of $\mathbf{A}$ given by

$$\overset{\triangledown}{\mathbf{A}} = -\frac{Y(\mathbf{A})}{\lambda}\left[f(\mathbf{A})\,\mathbf{A} - g(\mathbf{A})\,\mathbf{I} + \alpha(\mathbf{A}-\mathbf{I})^2\right]. \qquad 12.$$

This set of equations with $f(\mathbf{A}) = g(\mathbf{A}) = 1$ includes the UCM [$\alpha = 0$, $Y(\mathbf{A}) = 1$, $\eta_{\text{s}} = 0$], the Oldroyd-B [$\alpha = 0$, $Y(\mathbf{A}) = 1$], the Giesekus [$Y(\mathbf{A}) = 1$], and the simplified PTT models in the exponential [$\alpha = 0$, $Y(\mathbf{A}) = \exp[\varepsilon(\text{tr}\,\mathbf{A} - 3)]$] and linear [$\alpha = 0$, $Y(\mathbf{A}) = 1 + \varepsilon(\text{tr}\,\mathbf{A} - 3)$] variants. For the FENE-CR model of Chilcott & Rallison (1988), the functions are

$f(\mathbf{A}) = g(\mathbf{A}) = L^2/(L^2 - \text{tr}\,\mathbf{A})$, $\alpha = 0$, and $Y(\mathbf{A}) = 1$. This is a simplified FENE-type model without a molecular interpretation, as pointed out by Bird & Wiest (1995), but it is useful in the numerical study of the effects of elasticity without the complications introduced by a shear-thinning viscosity. Three usual variants of the FENE-P model are also contained in Equations 11 and 12 [with $\alpha = 0$ and $Y(\mathbf{A}) = 1$], which behave differently if L^2 is not large: $f(\mathbf{A}) = L^2/(L^2 - \text{tr}\,\mathbf{A})$ and $g(\mathbf{A}) = f_{\text{eq}}(\mathbf{A}) = L^2/(L^2 - 3)$ yield the original FENE-P of Bird et al. (1980) [$f_{\text{eq}}(\mathbf{A})$ refers to $f(\mathbf{A})$ at rest]; $f(\mathbf{A}) = (L^2 - 3)/(L^2 - \text{tr}\,\mathbf{A})$ and $g(\mathbf{A}) = f_{\text{eq}}(\mathbf{A}) = 1$ lead to the FENE-P used by Sureshkumar et al. (1997), where the relaxation time λ is only identical to the relaxation time of the other FENE-P models in the limit $L^2 \to \infty$; and a third alternative is $f(\mathbf{A}) = L^2/(L^2 - \text{tr}\,\mathbf{A})$ and $g(\mathbf{A}) = 1 \neq f_{\text{eq}}(\mathbf{A})$, as used by Housiadas & Beris (2003). FENE-type models involve a solvent as derived from kinetic theory, but $\eta_s = 0$ is admissible from the continuum mechanics perspective.

The common features of the stress and conformation tensor forms of the differential constitutive equations, which are at the source of numerical difficulties in handling viscoelastic fluid flows, are the absence of diffusion of the transported quantity ($\boldsymbol{\tau}_p$ or $\mathbf{A}$) and their reliance on the upper-convected derivative. In reality, there is always a very small amount of molecular diffusion of the polymer stress or of any structural quantity (El-Kareh & Leal 1989), but much smaller than necessary to stabilize the computations. Note also that the momentum equation lacks an explicit viscous diffusion term if the fluid description does not involve a contribution from a Newtonian-like solvent stress.

3. METHODS

The methods used to solve the governing differential equations, discussed in Section 2, are now described in the context of the FVM. For the FEM, the revision by Baaijens (1998) and the book by Owens & Phillips (2002) are recommended. Mathematical aspects of the rheological constitutive equations have been discussed by Joseph (1990) and Renardy (2000). Some of the points here considered are relevant irrespective of the discretization approach, be it FVM, FDM, FEM, or another.

3.1. Formulation of the Governing Equations

To formulate the governing equations, we first choose the most appropriate dependent variables, guided by some numerical criteria, and subsequently transform the original governing equations so that they are expressed in terms of those variables. Therefore, in this section we do not deal directly with physical issues but rather with numerical decisions based on criteria such as numerical stability, ease of application, computational efficiency, and robustness of procedures.

Regarding the equations of motion, most researchers follow the primitive variable formulation (velocity and pressure), but other formulations have been considered, namely the streamfunction/vorticity formulation, especially in the early days of CR (e.g., Perera & Walters 1977, Sasmal 1995). Recent works with variants of this formulation can still be found in two-dimensional (2D) simulations (Comminal et al. 2016, 2018).

Regarding the constitutive equation, having decided on the rheological model to use (from physical considerations), we then need to choose the best mathematical formulation to determine the fluid stress, anticipating solution by a numerical method. The basic choice of dependent variable is between the stress or the conformation tensor, leading to the corresponding stress or conformation formulations. Analytically they are equivalent, but the choice can have numerical implications and may also affect the way the momentum equation is written, since for each type of formulation several methods are possible, impacting differently on the final forms of both

governing equations. In the stress formulation, the choice of methods includes the original formulation, the elastic–viscous stress splitting (EVSS), the solvent–polymer stress splitting (SPSS), the both-sides diffusion (BSD), the adaptive viscoelastic stress splitting (AVSS), the explicitly elliptic momentum equation (EEME), the traceless stress tensor, and the reduced stress techniques. For the conformation tensor formulation, the choice is typically between some of the above techniques to solve for **A** in addition to the log-conformation (Fattal & Kupferman 2004), the square-root-conformation (Balci et al. 2011), or the kernel-conformation methods (Afonso et al. 2012c). Henceforth, we shall use the FENE-P or the Oldroyd-B models as prototypes, as they are building blocks in more complex constitutive equations.

3.1.1. Stress tensor formulation of the constitutive equation. The benefits of starting a discretization procedure from governing equations written in conservative form are well known (Roache 1972) and have been discussed in the context of viscoelastic flow simulations by Oliveira (2009). A conservative counterpart of the original FENE-P equation is given by

$$\boldsymbol{\tau}_p + \left(\lambda' \overset{\nabla}{\boldsymbol{\tau}}_p\right) = -\left(\eta'_p \overset{\nabla}{\mathbf{I}}\right) \;\Rightarrow\; \boldsymbol{\tau}_p + \left(\lambda' \overset{\nabla}{\boldsymbol{\tau}}_p\right) = 2\eta'_p \mathbf{S} - \frac{\mathrm{D}\eta'_p}{\mathrm{D}t}\mathbf{I}, \qquad 13.$$

which is equivalent to Equation 10, with $\lambda' \equiv \lambda / f(\boldsymbol{\tau}_p)$ and $\eta'_p \equiv a\eta_p / f(\boldsymbol{\tau}_p)$. However, it is difficult to guarantee that a discretized version of Equation 10 will reduce to a discretized version of Equation 13, thereby embodying the conservativeness properties of the latter. This generalized conservative property is a concern of discretization, not necessarily linked directly with conservation of a physical property. Strictly speaking, $\boldsymbol{\tau}_p$ is not conserved and Equation 10 is not a conservation equation, but sometimes arguments in the literature treat the conformation tensor, and indirectly the stress tensor, as a conserved property (e.g., Vaithianathan et al. 2006).

A different issue faced in the early days of CR was the necessity of identifying a diffusive term in the momentum equation, resulting from a stress (or part of the stress) behaving in a Newtonian way (having an instantaneous or nearly instantaneous relaxation response), even when the constitutive equations do not have any apparent Newtonian contribution. Such diffusive terms can be treated implicitly when the momentum equations are solved numerically, and since many flows relevant to viscoelasticity occur at low Reynolds number, the characteristic diffusion timescale is small, hence implying very small time steps if an explicit treatment of diffusion is adopted. Having a diffusive term in the momentum equation is thus very important to enhance numerical stability, to allow larger time steps in time-dependent simulations, and in general to increase the ellipticity of the momentum equation (King et al. 1988). This issue is well illustrated with the Oldroyd-B equation, whose original formulation (Oldroyd 1950) is given by Equation 8. In principle, the divergence of this total extra stress would be inserted in the momentum equation, resulting in a formulation without any apparent diffusive term. However, to provide numerical stability, one can decompose the total extra stress into the following sum of a viscous Newtonian, $\boldsymbol{\tau}_v = 2\eta_a \mathbf{S}$, and an elastic, $\boldsymbol{\tau}_e$, contribution:

$$\boldsymbol{\tau} = 2\eta_a \mathbf{S} + \boldsymbol{\tau}_e, \qquad 14.$$

where the added viscosity (η_a) needs to be defined. The first term, $2\eta_a \mathbf{S}$, is treated implicitly when solving numerically the momentum equation, and for the Oldroyd-B fluid, the elastic stress then in general satisfies

$$\boldsymbol{\tau}_e + \lambda \overset{\nabla}{\boldsymbol{\tau}}_e = 2\left(\eta_0 - \eta_a\right)\mathbf{S} - 2\left(\eta_a \lambda - \eta_0 \lambda_r\right)\overset{\nabla}{\mathbf{S}}. \qquad 15.$$

Depending on the choice of η_a, we identify the following three numerical techniques to deal with the stress: (*a*) EVSS uses $\eta_a = \eta_0$ ($\boldsymbol{\tau}_e$ from analytical manipulation: Equation 15 with the

appropriate modifications). This was proposed by Perera & Walters (1977) in the context of finite differences for second-order fluids, and by Rajagopalan et al. (1990) in the context of the FEM for the Giesekus, Oldroyd-B, and UCM models. (*b*) SPSS uses $\eta_a = \eta_s$, implying $\boldsymbol{\tau}_e = \boldsymbol{\tau}_p$, as naturally occurs when models having a Newtonian contribution are derived from kinetic theory, as in Equations 3 and 4. (*c*) In BSD, terms with a divergence of $-2\eta_a\mathbf{S}$ are added to both the left- and the right-hand sides of the momentum equation, with the former handled implicitly and the latter handled explicitly. BSD is most often used in conjunction with the SPSS formulation, with $\eta_a = \eta_p$ used in the added terms, but there are cases with $\eta_a = \eta_0$, and BSD can also be applied to the original Equation 8.

These possibilities have been discussed by Xue et al. (2004) and Amoreira & Oliveira (2010); in the context of the FEM, BSD was suggested by Guénette & Fortin (1995). Amoreira & Oliveira (2010) showed that if the remainder of the algorithm is coded exactly in the same way, then BSD is numerically equivalent to EVSS (as previously hinted by Alves et al. 2000). BSD is thus an easy way of achieving stability for steady-flow problems using implicit algorithms: The iterations required to equalize the added (implicit) and the subtracted (explicit) diffusive terms coincide with the outer iterations (or pseudo-time marching steps) in the overall algorithm. For unsteady flows, however, BSD requires excessive iterations within a time step, making the implicit algorithm inefficient, as shown by Amoreira & Oliveira (2010). If the added viscosity η_a is allowed to vary from 0 to η_0 for the simple start-up Poiseuille flow problem considered, they also showed that the most efficient formulation, in the sense of requiring a minimum total number of iterations, is achieved with SPSS—the natural way of introducing the stress in the momentum balance.

A somewhat different form of EVSS was introduced by Sun et al. (1996) termed AVSS, in which the added viscous term in the momentum equation is based on an artificial viscosity η_a that varies from point to point throughout the flow domain in a prescribed (empirical) way, being larger where the elastic stress dominates the viscous stress. The concept was applied with some success, with the given expression for the added viscosity incorporating both numerical and physical parameters ($\eta_a \approx h\tau_{max}/u_{max}$, where h is a typical cell spacing). Subsequently the viscosity expression has been refined (Sun et al. 1999), but it has remained basically empirical.

Another proposal for enhancing the numerical stability of the set of momentum and constitutive equations, based on pure mathematical manipulations, is the traceless stress tensor formulation of Oliveira (2000), where the fluid extra stress equation is rewritten into an equation for the evolution of the corresponding traceless tensor: $\boldsymbol{\tau}' = \boldsymbol{\tau} - \frac{1}{3}(\mathrm{tr}\boldsymbol{\tau})\mathbf{I}$ (alternatively, this change of variable can also be implemented with $\boldsymbol{\tau}_p$). In the momentum equation, the pressure is correspondingly modified to p' so that the transformed momentum equation reads as Equation 2 with $(p', \boldsymbol{\tau}')$ instead of $(p, \boldsymbol{\tau})$. Such transformation leads to a modified viscosity coefficient in the polymer constitutive equation, given by $\eta_p' \approx \eta_p[1 + \frac{1}{3}(\lambda/\eta_p)\mathrm{tr}\boldsymbol{\tau}_p]$ (or $\eta' = \eta_s + \eta_p'$ for a constitutive equation written in terms of the total stress), thus producing large viscosities in problematic regions of the flow domain where the trace of the original stress becomes very large (e.g., close to reentrant corners in contraction flows or other singular points in the domain). This traceless formulation was shown to require substantially fewer inner iterations to solve the pressure equation when applied to steady flows with an implicit sequential pressure-correction method [for which the pressure solution is the major numerical burden (e.g., Roache 1972)]. A difficulty associated with this formulation is that the traceless tensor, because of the way it is constructed, tends to develop large wall-normal normal stresses near a wall boundary (for example, it gives $\tau_{yy}' = -\frac{1}{3}\tau_{xx}$ for a wall aligned with the x-direction), and such normal stresses are difficult to implement correctly (and stably) numerically.

Finally, it is worth mentioning two methods in particular that have not yet attained widespread popularity. The first is the grid-by-grid method of Park & Lim (2010), which seems to be inspired

by the philosophy of algebraic Reynolds stress models in turbulence modeling, with the advective fluxes treated explicitly and evaluated locally and the stress equations inverted also locally (at node points) as a 3 × 3 matrix equation for the three stress components in 2D flows, (τ_{xx}, τ_{xy}, τ_{yy}). In three dimensions, the method becomes more complicated and requires inversion of local 6 × 6 matrices for the six stress components.

The second method is the natural stress formulation of Evans & Oishi (2017), inspired by Renardy (1994), in which the constitutive equation is solved in a local streamline/cross-stream coordinate system (defined by unit vectors $\hat{\mathbf{s}}$ and $\hat{\mathbf{n}}$, respectively). This method is particularly useful for alleviating problems of numerical diffusion, which are unavoidable with upwind-biased schemes unless the transported quantity is advected along the streamlines [as with the stress component τ_{ss} in this method, in which the stress tensor is decomposed in the local dyadic basis: $\boldsymbol{\tau} = \tau_{ss}\hat{\mathbf{s}}\hat{\mathbf{s}}^{\mathrm{T}} + \tau_{sn}(\hat{\mathbf{s}}\hat{\mathbf{n}}^{\mathrm{T}} + \hat{\mathbf{n}}\hat{\mathbf{s}}^{\mathrm{T}}) + \tau_{nn}\hat{\mathbf{n}}\hat{\mathbf{n}}^{\mathrm{T}}$]; this natural tensor formulation can similarly be applied to the conformation tensor (to be discussed in the next section), as in the work of Evans & Oishi (2017)]. Such a method is suitable, for example, to probe the stress behavior near singular points, and the authors have shown that it provides the correct trends on approaching the reentrant corner of a contraction flow, with a mesh much coarser than that utilized in similar studies by other authors. A possible drawback of this method when used in a general-purpose simulation code is the presence of terms divided by the velocity magnitude ($\|\mathbf{u}\|$) in the transformed constitutive equations, which arise from transformation to the local basis aligned with the streamlines (since the corresponding tangential unit vector is calculated as $\hat{\mathbf{s}} = \mathbf{u}/\|\mathbf{u}\|$); whenever the velocity approaches zero, such as at an internal stagnation point, the computations will diverge unless special care is taken. Extension to three dimensions is also challenging.

3.1.2. Conformation tensor formulation of the constitutive equation. In numerical terms, the final differential equations embedded in the general Equation 12 are not substantially different from the equations formulated for the stress tensor. Therefore, the methods for the $\boldsymbol{\tau}$ equations are essentially the same as for the $\mathbf{A}$ equations. The crucial difference is that $\mathbf{A}$ is by definition a positive-definite tensor, and preserving this property is important to guarantee numerical stability and ensure flow realizability. Hulsen (1990) proved analytically that $\mathbf{A}$ remains positive definite provided it was so initially for quite a general class of constitutive equations, which includes those here considered. Dupret & Marchal (1986) demonstrated that violation of this property during a numerical simulation leads to a Hadamard instability, with exponential growth of short–wave number components. Logarithm and square-root transformation formulations that intrinsically preserve the positive definiteness of $\mathbf{A}$ are discussed in Section 3.1.3. Vaithianathan & Collins (2003) have provided a very good introduction to the subject, and in fact these authors already hinted to the square-root formulation with their Choleski decomposition approach and commented on the logarithm approach as a technique to ensure positiveness on the evolution of the eigenvalues of $\mathbf{A}$.

3.1.2.1. Explicitly elliptic momentum equation formulation. In the EEME formulation, first described by Renardy (1985) and later derived and applied numerically by King et al. (1988), as examined from a current perspective with their positive-definite $\boldsymbol{\chi}$ tensor identified as $\boldsymbol{\chi} = (\eta_{\mathrm{p}}/\lambda)\mathbf{A}$ (cf. Owens & Phillips 2002), an analytical manipulation of the evolution equation for $\boldsymbol{\chi}$ is made by applying the divergence operator to the whole constitutive equation for the UCM model, $\nabla \cdot \boldsymbol{\tau} = -\lambda \nabla \cdot \overset{\nabla}{\boldsymbol{\chi}}$, and substituting the result back into the momentum equation. The procedure mimics the steps taken to solve the equations analytically when that is possible. For the UCM model

($\eta \equiv \eta_p$), such manipulation gives rise to a momentum equation having an explicit diffusion term,

$$0 = -\nabla q + \lambda \nabla \cdot (\boldsymbol{\chi} \cdot \nabla \mathbf{u}) + \lambda \nabla \mathbf{u} \cdot (\nabla \cdot \boldsymbol{\chi}), \qquad 16.$$

for steady-state, inertialess flow conditions, where the first term on the right-hand side is the pressure gradient (applied to a substantial pressure, $q = p + \lambda \mathbf{u} \cdot \nabla p$), the second term includes diffusion, and the third term is a new term. For other situations, the reformulation becomes rather complex. In this transformed equation, the normal diffusion terms that are aligned with the independent spatial coordinates are treated implicitly as an anisotropic viscous contribution (provided $\chi_{11} > 0$ and $\chi_{22} > 0$ in two dimensions), while the off-diagonal diffusive terms (multiplied by χ_{12}) and the new term are treated explicitly.

3.1.2.2. Stress diffusion. As discussed below, one way of achieving numerical stability in the calculation of the evolution of the conformation tensor at high Reynolds and Weissenberg numbers, especially when using spectral-like approximations to the spatial derivatives, is to add a diffusion term to Equation 12 for the FENE-P model (Thomases 2011):

$$\overset{\nabla}{\mathbf{A}} = -\frac{1}{\lambda}\left[f(\mathbf{A})\mathbf{A} - g(\mathbf{A})\mathbf{I}\right] + \kappa \nabla^2 \mathbf{A}. \qquad 17.$$

Here κ is the coefficient of stress diffusivity, prescribed nondimensionally via a Schmidt number, $Sc = (\eta_0/\rho)/\kappa$, and the original FENE-P model is recovered in the limit $Sc \to \infty$. As discussed at the end of Section 2, a physically based stress diffusion term makes sense; alternatively, its inclusion is equivalent to a modification of the constitutive modeling, which may be considered here as a valid reformulation for improving the numerical stability, provided it does not entail significant changes to the flow physics.

The initial successful stabilization in the first direct numerical simulations (DNS) of wall turbulence with viscoelastic models used a certain amount of physical stress diffusion, with Sc varying from 0.1 to 1 (Sureshkumar & Beris 1995). Even though this changed the constitutive equation, their linear stability analysis of channel Poiseuille flow of Oldroyd-B fluids showed a negligible influence on the critical eigenmodes and a significant influence on the singular eigenmodes, while no numerical instabilities were observed in the full 3D high–Reynolds number flow calculations. Therefore, a wealth of research on drag reduction by polymer additives in fully developed wall turbulent flows pursued this approach, with Sureshkumar et al. (1997) making one of the first contributions in this area. Although such numerical results of turbulent drag reduction in polymer solutions compare qualitatively well with experimental data of the first and second moments of the velocity, a more detailed analysis of turbulent phenomena shows that some results are affected by stress diffusion, especially at small and intermediate scales, as recently shown by Gupta & Vincenzi (2018) for elastic turbulence conditions.

3.1.2.3. Boundedness of tr A. Vaithianathan & Collins (2003) first proposed an interesting technique to prevent the FENE-P molecular model extending above the prescribed maximum extensibility [mathematically, tr $\mathbf{A}$ is less than L^2; otherwise $f(\mathbf{A})$ grows to infinity in the limit tr $\mathbf{A} \to L^2$ and eventually becomes negative for tr $\mathbf{A} > L^2$, leading to nonphysical results]; their technique was refined by Dubief et al. (2005) and Richter et al. (2010). The technique basically consists of deriving an equation for the evolution of tr $\mathbf{A}$ by contracting indices in Equation 12 for the FENE-P model [$\alpha = 0, Y(\mathbf{A}) = 1, g(\mathbf{A}) = 1$] and solving it for the denominator of the $f(\mathbf{A})$ function algebraically after discretization. For example, with Euler's explicit scheme, a quadratic equation for $f^{-1} = 1 - \text{tr}\,\mathbf{A}/L^2 > 0$ is obtained,

$$(f^{-1})^2 - bf^{-1} - c = 0, \qquad 18.$$

with a single positive real solution that guarantees tr $\mathbf{A} < L^2$ (see Richter et al. 2010).

Following Richter et al. (2010), this value of $f^{-1}(\mathbf{A})$ is retained unchanged during the time advancement of the six conformation tensor components for the current time step [even if, at the end of the time step, tr $\mathbf{A}$ from the updated components differs from tr $\mathbf{A}$ in the fixed $f^{-1}(\mathbf{A})$ used to update them], thus effectively bounding the maximum value of tr $\mathbf{A}$ by L^2. It is tempting to imagine that a technique of the same type can be devised to guarantee that the eigenvalues of $\mathbf{A}$ are positive, $\lambda_i > 0$, instead of using the logarithm formulation described in the next section.

Another technique to bound tr $\mathbf{A} < L^2$, suggested by Vaithianathan & Collins (2003), was later retaken by Housiadas et al. (2010): While $\mathbf{A}$ is bound by the above limit, a modified tensor $\hat{\mathbf{A}} = f(\mathbf{A})\mathbf{A}$ is unbounded. By transforming the governing equations from $\mathbf{A}$ to $\hat{\mathbf{A}}$, transforming again to solve for $\log\hat{\mathbf{A}}$ (natural logarithm), and limiting the maximum attainable value of $\log\hat{\mathbf{A}}$ so that its Frobenius norm becomes smaller than a specified limit ($\|\log\hat{\mathbf{A}}\|_{\mathrm{F}} \leq M$), Housiadas et al. (2010) developed a code for turbulence of dilute polymer solutions that was shown to be more robust than their previous unbounded code (in terms of avoiding overflows when $\hat{\mathbf{A}}$ or $\log\hat{\mathbf{A}}$ is too large).

3.1.3. Log-conformation and other transformations. Instead of solving the evolution Equation 12 for the conformation tensor $\mathbf{A}$, it is preferable to use a related tensor displaying smoother behavior than $\mathbf{A}$. Since $\mathbf{A}$ is symmetric and positive definite, it has real eigenvalues and is readily diagonalized [$\tilde{\mathbf{A}} = \mathbf{R}^{\mathrm{T}}\mathbf{A}\mathbf{R} = \mathrm{Diag}(\lambda_1, \lambda_2, \lambda_3)$, where $\mathbf{R}$ is a rotation matrix formed with the eigenvectors of $\mathbf{A}$]; hence, a suitable scalar function can operate on the three positive diagonal values λ_i, such as the natural logarithm. Fattal & Kupferman (2004) demonstrated that the velocity gradients may be decomposed as $\nabla\mathbf{u}^{\mathrm{T}} = \boldsymbol{\Omega} + \mathbf{B} + \mathbf{N}\mathbf{A}^{-1}$, where $\boldsymbol{\Omega}$ and $\mathbf{N}$ are antisymmetric tensors and $\mathbf{B}$ is symmetric and commutes with $\mathbf{A}$. Such decomposition permits an easy transformation of Equation 12 to a form for the evolution of the natural logarithm of the conformation tensor ($\boldsymbol{\psi} \equiv \log\mathbf{A}$):

$$\frac{\mathrm{D}\boldsymbol{\psi}}{\mathrm{D}t} - (\boldsymbol{\Omega}\boldsymbol{\psi} - \boldsymbol{\psi}\boldsymbol{\Omega}) - 2\mathbf{B} = -\frac{Y(\mathrm{e}^{\boldsymbol{\psi}})\mathrm{e}^{-\boldsymbol{\psi}}}{\lambda}\left[f(\mathrm{e}^{\boldsymbol{\psi}})\mathrm{e}^{\boldsymbol{\psi}} - g(\mathrm{e}^{\boldsymbol{\psi}})\mathbf{I} + \alpha\left(\mathrm{e}^{\boldsymbol{\psi}} - \mathbf{I}\right)^2\right]. \qquad 19.$$

An advantage is the transformation of the expected exponential and abrupt variations of the stress, and of the conformation fields, in flows with singular points or other complexities, into quasi-linear and smoother variations, which are much more amenable to be approximated by standard numerical methods with adequate accuracy and stability. In a second paper, Fattal & Kupferman (2005) described in more detail the motivations and advantages of their method and provided numerical results for the lid-driven cavity benchmark flow, using an FDM. One key point of the log-conformation approach, which is now largely favored in terms of allowing stable calculations at high Weissenberg numbers, is its ability to guarantee by construction a positive-definite conformation tensor. Since the conformation tensor, and indirectly the extra stress, is obtained by exponentiation of the log-conformation tensor, which is an operation performed on the principal axes of the tensors, $\tilde{\mathbf{A}} = \exp(\tilde{\boldsymbol{\psi}})$, one must have $\lambda_i \geq 0$ (obtaining the log-conformation tensor from $\mathbf{A}$ is also performed on principal axes). The decomposition employed in the log-conformation method has conceptual similarities to the continuous eigendecomposition method of Vaithianathan & Collins (2003), which is designed to achieve positive definiteness of $\mathbf{A}$. In their method, the conformation tensor is eigendecomposed into independent equations for the eigenvalues and eigenvectors, which are separately evolved in time and subsequently used to reconstruct the new conformation tensor field. However, these authors did not transform the equation to solve for $\log\mathbf{A}$, and even though their method ensured that the sum of the eigenvalues remained limited by L^2 (see previous subsection), it did not guarantee that the individual eigenvalues remained positive. In a second method proposed in the same paper, Vaithianathan & Collins used a Cholesky decomposition of

NUMERICAL COMPARISON OF STRESS/CONFORMATION TENSOR FORMULATIONS

In the **Supplemental Appendix**, we provide the differential evolution equations that are implemented in codes for the simulation of the time-dependent start-up channel flow of viscoelastic fluids obeying the FENE-P model, which can be used to assess the accuracy and numerical efficiency of five of the formulations discussed here: stress, reduced stress, standard-conformation, log-conformation, and square-root-conformation. The **Supplemental Appendix** includes a comparison of results and the Fortran codes are available at **http://www.fe.up.pt/~fpinho/research/annurev.html**.

Supplemental Material >

A that guarantees positive eigenvalues when the logarithm of the diagonal values of the matrix are evolved in time, but they did not pursue this idea in subsequent works (Vaithianathan et al. 2006).

Variants of the original log-conformation method, for instance, by Saramito (2014) and Knechtges et al. (2014), have shown good stability to deal with difficult viscoelastic flows, but within their specific limits. In several studies (e.g., Afonso et al. 2009, 2011; Palhares et al. 2016; Pimenta & Alves 2017), the log-conformation formulation was found to offer similar accuracy to the standard stress formulation for complex flows. The transformation of the conformation tensor to logarithm scale seems to enhance precision in regions of exponential growth of the stress field.

Other formulations have been devised to promote numerical stability of viscoelastic flow calculations; in particular, we mention the square-root-conformation tensor approach of Balci et al. (2011), which also guarantees a positive-definite **A**. Lozinski & Owens (2003) showed earlier that the use of the square root of the conformation tensor could ensure the positive definiteness of both the square-root- and the original-conformation tensor (please see the sidebar titled Numerical Comparison of Stress/Conformation Tensor Formulations). This transformation has the advantage over the logarithm formulation of relying on a simpler set of equations not requiring the computation of the eigenvalues/eigenvectors of **A**. Therefore, the computing time to update the conformation tensor can be smaller than with the log conformation. However, since the major effort in an FVM flow code is typically solving the pressure equation, the gain in efficiency by the square-root formulation may not be very high. In terms of stability, our experience is that the log formulation has an edge over the square-root formulation, as it allows higher Wi to be reached (cf. Afonso et al. 2012c, Palhares et al. 2016), but further comparative research on stability, efficiency, and accuracy is needed.

Afonso et al. (2012c) generalized these methods by devising the so-called kernel-conformation method, later rediscovered by Niethammer et al. (2018). The numerical properties of a specific matrix-transformation formulation depend on the chosen kernel function in the integral transformation formula relating **A** to $\boldsymbol{\psi}$. In this sense, the kernel-conformation approach will not in general ensure by design that all transformations will lead to stable numerical methods. However, some kernel functions like the linearly shifted kernel, the $\log_a$, the double logarithm, the k-th root, and the inverse hyperbolic sine resulted in significant improvement of high–Weissenberg number calculations for the confined cylinder flow benchmark (Afonso et al. 2012c). The excessive sublinearization of some kernel functions led to numerical problems, and in the end, the best functions were the logarithms using small bases ($a < 10$) and the k-th root with $-16 \leq k \leq -2$—hence including both the classic log- and square-root-conformation functions.

3.2. Discretization

In the standard FVM the differential equations governing the flow of a viscoelastic fluid, given in Section 2, are integrated over small control volumes (cells) forming the computational mesh and, with the help of simple interpolation profiles, are transformed into sets of linearized algebraic equations. Although the original equations are nonlinear, namely by the presence of advective terms in the momentum equations and the stress function $Y(\boldsymbol{\tau}_\mathrm{p})$ in Equation 5 and $f(\boldsymbol{\tau}_\mathrm{p})$ in Equation 10, in standard FVM an a priori linearization is performed to transform the discretized equations into sets of linearized equations. The underlying nonlinearities are dealt with by Picard-type iteration (see Section 3.3). This process corresponds to the discretization of the problem and it is advantageous to employ schemes that guarantee an accuracy of at least second order in terms of the discretization error (Ferziger & Perić 2002) while preserving numerical stability. When the central node in a cell is denoted by index P and the neighboring node through face f over a generic control volume is denoted by index F, upon integration using Gauss's divergence theorem and the midpoint rule for integration over both a cell face area ($\boldsymbol{\mathcal{A}}_f$) and a cell volume ($V_\mathrm{P}$), the momentum equation becomes (more details given by Oliveira et al. 1998)

$$\rho V_\mathrm{P}\left(\frac{\partial \mathbf{u}}{\partial t}\right)_\mathrm{P} + \sum_f F_f \mathbf{u}_f - \sum_f D_f\,(\mathbf{u}_\mathrm{F} - \mathbf{u}_\mathrm{P}) = -V_\mathrm{P}(\nabla p)_\mathrm{P} + \sum_f \boldsymbol{\mathcal{A}}_f \cdot \boldsymbol{\tau}_f + \mathbf{S}_\mathbf{u}; \qquad 20.$$

the continuity equation (for constant ρ) is given by

$$\sum_f F_f = 0\,, \text{ with } F_f = \rho \boldsymbol{\mathcal{A}}_f \cdot \mathbf{u}_f; \qquad 21.$$

and the FENE-P constitutive Equation 13 is written as

$$V_\mathrm{P}\boldsymbol{\tau}_\mathrm{P} + V_\mathrm{P}\left(\lambda' \frac{\partial \boldsymbol{\tau}}{\partial t}\right)_\mathrm{P} + \sum_f \frac{1}{\rho} F_f (\lambda' \boldsymbol{\tau})_f = \lambda'_\mathrm{P}\left(\boldsymbol{\tau}\cdot\nabla\mathbf{u} + \nabla\mathbf{u}^\mathrm{T}\cdot\boldsymbol{\tau}\right)_\mathrm{P} V_\mathrm{P} + \eta'_\mathrm{P}\left(\nabla\mathbf{u} + \nabla\mathbf{u}^\mathrm{T}\right)_\mathrm{P} V_\mathrm{P} + \mathbf{S}_\boldsymbol{\tau}. \qquad 22.$$

In these equations, F_f is the outward mass flow rate through cell face f, and $D_f = (\eta_\mathrm{s})_f \mathcal{A}_f / d_f$ is the diffusion flux at cell face f. The cell-face area vector is defined pointing outward, i.e., $\boldsymbol{\mathcal{A}}_f = \mathcal{A}_f \mathbf{n}$; the scalar face area is $\mathcal{A}_f = \sqrt{\boldsymbol{\mathcal{A}}_f \cdot \boldsymbol{\mathcal{A}}_f}$; and the projected distance between neighboring nodes is $d_f = \boldsymbol{\mathcal{A}}_f \cdot \mathbf{d}_f / \mathcal{A}_f$, with $\mathbf{d}_f = \mathbf{r}_\mathrm{F} - \mathbf{r}_\mathrm{P}$. The so-called source terms $\mathbf{S}_\mathbf{u}$ and $\mathbf{S}_\boldsymbol{\tau}$ contain terms not explicitly shown. For example, $\mathbf{S}_\mathbf{u}$ in Equation 20 contains contributions from the discretization of (*a*) some parts of $\nabla \cdot \eta_\mathrm{s} \nabla \mathbf{u}^\mathrm{T}$, if for some reason η_s is variable (e.g., through temperature dependence); (*b*) $\nabla \cdot \eta_\mathrm{s} \nabla \mathbf{u}$, namely from the cross-derivative contributions due to the use of nonorthogonal meshes (cf. Oliveira et al. 1998); (*c*) other terms such as $\rho V_\mathrm{P} \mathbf{g}$; and (*d*) the advective flux due to deferred correction treatment of high-resolution schemes (cf. Alves et al. 2001). The term $\mathbf{S}_\boldsymbol{\tau}$ in Equation 22 contains the term with the material derivative of η'_p in the FENE-P equation, $-[V_\mathrm{P}\partial(\eta'_\mathrm{p})_\mathrm{P}/\partial t + \sum_f \frac{1}{\rho} F_f (\eta'_\mathrm{p})_f]\mathbf{I}$; higher-order contributions to the advective stress fluxes, $-\sum_f \frac{1}{\rho} F_f (\lambda' \boldsymbol{\tau})_f$ (see Section 3.2.1); and additional terms present in some constitutive equations (e.g., terms multiplied by ξ and α in Equation 5 for the PTT and Giesekus models, respectively). Typically, in an implicit FVM solution algorithm, the terms written on the left-hand side of Equations 20 and 22 are calculated implicitly, and those on the right-hand side explicitly, when one solves the discretized forms of these equations as a matrix system. Either Equation 20 or 22 is then written, after linearization, as

$$a^\phi_\mathrm{P}\phi_\mathrm{P} - \sum_\mathrm{F} a^\phi_\mathrm{F}\phi_\mathrm{F} = b^\phi \;\Rightarrow \mathbf{A}^\phi \cdot \boldsymbol{\phi} = \mathbf{b}^\phi, \qquad 23.$$

where a^ϕ_P and a^ϕ_F are the components of the square $N_\mathrm{c} \times N_\mathrm{c}$ matrix $\mathbf{A}^\phi$ (N_c is the total number of cells in the mesh), each incorporating advection and diffusion contributions, and the column

matrix $\mathbf{b}^{\phi}$ contains the remaining terms, which are treated explicitly for any of the dependent variables ($\phi = \mathbf{u}, p, \boldsymbol{\tau}_{\mathrm{p}}$). Parts of the advective fluxes, however, are also treated explicitly (see Section 3.2.1). The constraint imposed by the continuity Equation 21 provides a Poisson equation for pressure or pressure correction (depending on the algorithm chosen; see Ferziger & Perić 2002).

The equations given above are valid for both structured and unstructured grids, the difference being the number of faces considered in the summations; for structured grids of hexahedral cells, f varies from 1 to 6, while for unstructured meshes the range of f can vary from cell to cell. Another difference is that the velocity gradients, which appear in the momentum equation through the viscous stresses and in the constitutive equation, can be simply represented with nonorthogonal geometries in a structured mesh using a coordinate transformation, $(\nabla \mathbf{u})_{ij} = \partial u_j/\partial x_i = (\beta_{li}/J)\partial u_j/\partial \xi_l$, where J is the Jacobian of the coordinate transformation and β_{li} are metric coefficients related to area components of the cells (cf. Oliveira et al. 1998 or Ferziger & Perić 2002 for details). Several variants are also available for unstructured meshes, with more or fewer degrees of complexity (see Ferziger & Perić 2002). Notice also that the viscous term treated implicitly in Equation 20, which is multiplied by D_f, is the so-called direct diffusion flux, $\eta_{\mathrm{s}}(\nabla \mathbf{u}^{\mathrm{T}})_f \cdot \mathbf{d}_f$, while the remaining terms are included in the source term $\mathbf{S}_{\mathbf{u}}$.

Unstructured methodologies for viscoelastic flows using cell-centered control volumes similar to those used here, but in the context of variable-mesh topology, have been developed by Edussuriya et al. (2004), with an iterative time-dependent solver for multiphysics applications, and by Pimenta & Alves (2017) for a general-purpose open-source software. Different mesh structures have also been considered, such as the dual-mesh approach (Sahin & Wilson 2007), in which the velocities are stored at the vertices of a mesh element (akin to FEM discretization) and the stresses at their centers, with momentum conservation enforced on the dual-mesh control volume formed around each element vertex. Two issues that are very important when devising accurate and stable numerical methods for viscoelastic fluid flow simulations are discussed in the next two sections.

3.2.1. Higher-order advective schemes. One issue associated with the hyperbolic-type constitutive equation for the stress, or for a structure tensor, is the absence of a diffusion-like term in the equation and the need to employ approximation schemes for advection that are more accurate than the basic upwind differencing scheme. This first-order scheme is the most stable but is known to introduce excessive numerical diffusion, as shown in many studies, especially with rheological models that do not have a solvent contribution such as the UCM (Alves et al. 2000); therefore, better alternatives are required.

The advective flux of a generic variable ϕ (which might be a velocity component or a stress/conformation/log-conformation tensor component, that is, $\phi = u_i$, τ_{ij}, A_{ij}, or ψ_{ij}) at a finite-volume cell face f can be decomposed into a pure upwind contribution ϕ^{up} and a correction $\Delta\phi$ that guarantees higher-order accuracy and TVD (total variation diminishing) properties of the advection scheme:

$$F_f\phi_f = F_f^+\left(\phi_f^{\mathrm{up}+} + \Delta\phi_f^+\right) + F_f^-\left(\phi_f^{\mathrm{up}-} + \Delta\phi_f^-\right) = F_f\left(\phi_{\mathrm{C}} + \Delta\phi_f^{\pm}\right). \qquad 24.$$

If the mass flux is positive [$F_f^+ \equiv \mathrm{Max}(F_f, 0) = F_f$], the upwind value of ϕ is $\phi_f^{\mathrm{up}+} = \phi_{\mathrm{P}}$, and if the flux is negative [$F_f^- \equiv \mathrm{Min}(F_f, 0) = F_f$], the upwind value is that of the neighboring cell F: $\phi_f^{\mathrm{up}-} = \phi_{\mathrm{F}}$. The corresponding corrections ($\Delta\phi_f^{\pm}$) depend on the advection scheme employed. With the CUBISTA [convergent and universally bounded interpolation scheme for the treatment of advection (Alves et al. 2003a)] scheme they are

$$\frac{\Delta\phi_f^{\pm}}{\phi_{\mathrm{D}} - \phi_{\mathrm{U}}} = \mathrm{Max}\left[0, \mathrm{Min}\left[\tfrac{3}{4}\tilde{\phi}_{\mathrm{C}}, \tfrac{3}{8} - \tfrac{1}{4}\tilde{\phi}_{\mathrm{C}}, \tfrac{3}{4} - \tfrac{3}{4}\tilde{\phi}_{\mathrm{C}}\right]\right], \qquad 25.$$

written in terms of normalized variables, $\tilde{\phi}_C = (\phi_C - \phi_U)/(\phi_D - \phi_U)$, where indices C, D, and U respectively mean central, downwind, and upwind nodal values, which depend on the sign of F_f. Similar expressions can be obtained for other high-resolution schemes, such as the SMART (sharp and monotonic algorithm for realistic transport) scheme of Gaskell & Lau (1988).

Alves et al. (2003a) demonstrated that the CUBISTA scheme provides second-order accuracy (third order in the best scenario) while maintaining bounded values (ϕ_f will remain between ϕ_P and ϕ_F) and improved iterative convergence properties. They showed that while other popular advective schemes may not converge efficiently, when applied to typical benchmark problems in viscoelastic fluid flow simulations, the CUBISTA scheme can provide good iterative convergence.

The idea behind the decomposition of Equation 24 is that the upwind bias keeps the numerical scheme robust and stable. This preconception was so strong that most of the earliest numerical procedures were rooted on upwind differences, not only for the velocity components in the momentum equations, but more so for the stress components in the constitutive equations. However, various works have demonstrated that such forms of basic upwind should be avoided, as the inherent numerical diffusion is so strong that it results in clear erroneous predictions of important flow structures (cf. figure 19 of Alves et al. 2003a). The natural stress formulation discussed in Section 3.1.1 (Evans & Oishi 2017) provides an alternative way of mitigating numerical diffusion in the stress equation.

Other high-resolution schemes have been employed with specific purposes, for example, to ensure positiveness of the advected variable. The turbulence community's early concerns about added stress diffusion for stability prompted Vaithianathan et al. (2006) to address the issue without changing the rheological constitutive equation; instead, they adopt an extension of the original Kurganov & Tadmor (2000) second-order bounded scheme to deal with tensor quantities in order to ensure that symmetric positive-definite tensors, like $\mathbf{A}$, would remain so everywhere. In this method, the advection of $\mathbf{A}$ in the original constitutive equation is approximated by a modified central differencing scheme with boundedness based on flux limiters. The resulting scheme has arbitrary order in time and second order in space except at points where loss of positive definiteness requires switching to a first-order scheme. The method has been used successfully for turbulent flows of FENE-P fluids, namely in isotropic turbulence (Vaithianathan et al. 2006, Valente et al. 2014, Ferreira et al. 2016), in homogeneous shear with polymer mixing (Vaithianathan et al. 2007), and in elastic turbulence (Gupta & Vincenzi 2018). Usually the conformation tensor equation is discretized with finite differences, combined with spectral methods in periodic directions for the remaining governing equations.

3.2.2. Stress–velocity coupling. Another term in the discretization that needs particular attention is the traction force in the momentum equation, which results from the representation of the stress divergence. In FVM it is well known that the face velocity (at a cell boundary between two computational cells) in the mass flux cannot simply be given by a linear interpolation of velocity components from neighboring cells, as that may lead to oscillations and velocity–pressure decoupling. As explained by Ferziger & Perić (2002), a corrective dissipative term can dampen such oscillations, an idea further explored by Oliveira et al. (1998) for viscoelastic fluids.

An important term in viscoelastic models is the traction force balance at the cell faces of the momentum equation, $\sum_f \mathbf{T}_f = \sum_f \boldsymbol{\mathcal{A}}_f \cdot \boldsymbol{\tau}_f$ (cf. Equation 20). In order to avoid stress–velocity decoupling, the cell face stress required in the stress divergence also requires a specific interpolation, as originally discussed by Oliveira et al. (1998) and further developed by Afonso et al. (2012a). The expression for the traction vector, $\mathbf{t} = \mathbf{n} \cdot \boldsymbol{\tau}$, at any cell face f with outward unit-normal $\mathbf{n}$,

taking into account only the main part of the stress-velocity coupling term, is of the type:

$$\mathbf{t}_f = \overline{\mathbf{t}}_f + \left(\frac{\frac{\lambda}{\Delta t}}{1+\frac{\lambda}{\Delta t}}\right)\left(\mathbf{t}_f^n - \overline{\mathbf{t}}_f^n\right) + \left(\frac{\eta_\mathrm{p}}{1+\frac{\lambda}{\Delta t}}\right)\left\{\left(\frac{\partial \mathbf{u}}{\partial n}\right)_f - \left(\overline{\frac{\partial \mathbf{u}}{\partial n}}\right)_f + \mathbf{n}\left[\left(\frac{\partial u_\mathrm{n}}{\partial n}\right)_f - \left(\overline{\frac{\partial u_\mathrm{n}}{\partial n}}\right)_f\right]\right\}. \quad 26.$$

At steady state, we have $\mathbf{t}_f = \mathbf{t}_f^n$ and $\overline{\mathbf{t}_f} = \overline{\mathbf{t}_f^n}$ (superscript n is the previous time level, while the absence of a superscript means a new time level $n+1$), and the traction at the face becomes equal to the linearly interpolated value (indicated by the overbar) plus a corrective term (in curled brackets) proportional to Δx^2 times third derivates of velocity (since $\mathbf{u}'_f \approx \overline{\mathbf{u}}'_f - \frac{1}{8}\Delta x^2 \mathbf{u}'''_f$), which act so as to cancel oscillations of wavelengths twice the cell size Δx. It is worth exploring application of the above expression to any differential constitutive equation, following either the stress or the conformation formulations; all it needs is the stress components at cell centers (in Equation 26 it is possible to use λ', η'_p instead of λ, η_p for consistency with nonlinear models such as the FENE-P or PTT, but this may have the unwanted effect of reducing too much the magnitude of the corrective dissipation term). Pimenta & Alves (2017) proposed a different stress–velocity coupling based on similar ideas, which is currently used in the rheoTool library (Pimenta & Alves 2016).

3.2.3. Wall boundary conditions. Inspection of the constitutive Equation 22 indicates that the stress is not required at a wall boundary, since the no-slip and no-penetration assumptions yield $F_f = 0$ (here f denotes a wall face). Nevertheless, a boundary condition for the stress is still needed at the wall for the traction term in the momentum Equation 20.

In steady-flow problems, with constitutive equations having a zero second normal stress difference coefficient (e.g., FENE-P, or PTT with $\xi = 0$), the assumption of a local linear flow near the walls is appropriate (implying a tangential traction given by $\mathbf{t}_\mathrm{t} = \eta_\mathrm{p}\partial \mathbf{u}_\mathrm{t}/\partial n$, with $\mathbf{u}_\mathrm{t} = \mathbf{u} - u_\mathrm{n}\mathbf{n}$ and $u_\mathrm{n} = \mathbf{u}\cdot\mathbf{n}$, where subscripts n and t refer to directions normal and tangential to the wall, respectively) (Oliveira et al. 1998, Xue et al. 1998).

For unsteady viscoelastic problems, the linear velocity assumption at a no-slip wall leads to erroneous solutions, as seen even in planar Poiseuille start-up flow (Duarte et al. 2008). The tangential stress component will be time varying and the corresponding local time variation term, $\lambda\partial\tau_{xy}/\partial t$, must be added to the Couette component, $\eta_\mathrm{p}\partial u/\partial y$, for a wall aligned with x. The analytical solution of Waters & King (1970) is useful to assess the correct implementation of the boundary condition. Thus, in general, with collocated meshes, two strategies have been followed: (*a*) Obtain the wall stress from the momentum equation evaluated at the wall assuming zero advection (Duarte et al. 2008), and (*b*) extrapolate the necessary stress components to the wall from their values at the adjacent nodes. Strategy *b* is simpler and more general, and although there is no theoretical work so far to justify it, the technique has been adopted with success in several works (Habla et al. 2012, Sousa et al. 2016, Pimenta & Alves 2017). Some authors impose a zero gradient normal to the walls, which is not correct even in fully developed flows, but the error introduced is local and does not seem to significantly affect the global solution.

With some types of staggered meshes, with both velocity components and shear stress components staggered relative to the center of cell position, such as in the works of Darwish et al. (1992), Mompean & Deville (1997), and Phillips & Williams (1999)—these last authors have provided an interesting discussion on the subject of mesh arrangement—and if in addition the velocity nodes are located right at the wall face (a practice not followed by those authors), there is no need to evaluate the tangential stress component at a wall boundary.

However, for the momentum equation normal to a wall boundary, the normal traction vector is needed: It is zero for constitutive models with null second normal stress difference, and otherwise, in that type of mesh [designated the first mesh system by Roache (1972)] it is calculated as part of

the overall solution, whereas for collocated meshes it can be obtained with strategy *b* above. The time is right for a more systematic investigation of the advantages, shortcomings, and accuracy of both types of mesh for complex flows of viscoelastic fluids.

3.3. Algorithm

We focus our review of algorithmic aspects of non-Newtonian viscoelastic fluid calculations on time-dependent flows, as these are becoming increasingly important, and methods for steady-state flow calculations may be seen as particular cases. There are two main approaches to computing time-dependent viscoelastic flows, which are discussed next: (*a*) iterative-solution methods and (*b*) fractional-step methods.

3.3.1. Iterative methods. When the time derivatives in the semidiscretized Equations 20 and 22 given in the previous section are represented with, for example, the backward difference formula, then the governing equations for momentum transport, mass conservation (a Poisson equation for pressure or pressure correction), and the constitutive equation are solved several times, normally in a sequential way, to advance the solution from time t^n to time $t^{n+1} = t^n + \Delta t$. The number of iterations at each time step (Δt) may be large when the time step itself is large, the interlinks between equations are stiff, or the nonlinearities are important. For example, for a viscoelastic vortex shedding problem at moderate Reynolds number ($Re \approx 100$), about three to four outer iterations were sufficient for the normalized residuals of the equations to become smaller than 10^{-2} (Oliveira 2001). In recent calculations by Oliveira (2017), with normalized residuals of about 10^{-4}, the number of outer iterations rose to about 10 or higher, with the possibility of divergence within a time step.

Some of the authors mentioned in the next subsection employ fractional-step methods together with iteration, e.g., Richter et al. (2010), Housiadas et al. (2010), D'Avino et al. (2012) (for some of the schemes proposed, namely the Gear implicit and the Crank–Nicolson), and Castillo & Codina (2015) (who refer to the need for 9–13 outer iterations for a lid-driven cavity flow problem).

3.3.2. Fractional-step methods. Fractional-step and projection methods have been widely applied in Newtonian fluid mechanics (Chorin 1968, Kim & Moin 1985, Perot 1993), and when the temporal discretization is semi-implicit, they do not require iteration within a time step, a major advantage in terms of efficiency for unsteady flow calculations (see Ferziger & Perić 2002, p. 181). To this end, the linear terms in any of the governing equations are approximated implicitly using the second-order Crank–Nicolson scheme, and the nonlinear terms are treated explicitly, in a deferred correction way, using, for example, the Adams–Bashforth scheme, which is also second-order accurate in time. Other options are viable, such as a backward differentiation discretization of the time derivative terms, a second-order extrapolation of advective terms in both the motion and constitutive equations (akin to the Adams–Bashforth scheme) and of the deformation terms in the constitutive equations only, and a fully implicit discretization of viscosity Laplacian and relaxation terms. Perot (1993) dealt with the issue that the original fractional-step method implied a time-splitting error of first order in Δt and showed how second-order accuracy could be achieved by making an analogy with block lower–upper decomposition. Since then, several studies have demonstrated the second-order temporal accuracy of improved fractional-step methods, including the case of viscoelastic non-Newtonian computations, as discussed next. The gains in computational efficiency make fractional-step semi-implicit methods highly attractive for unsteady viscoelastic simulations provided numerical stability is not too compromised (Fiétier & Deville 2003, van Os & Phillips 2004). Such methods are particularly suitable for orthogonal Cartesian meshes

and are often applied to simulate some turbulent flows [e.g., DNS or LES (large eddy simulation) in a rectangular domain with periodic boundary conditions, using time steps much smaller than those imposed by the CFL (Courant–Friedrichs–Lewy) condition (Vaithianathan & Collins 2003, Dubief et al. 2005, Housiadas et al. 2010, Richter et al. 2010), presumably due to stability considerations and the need to resolve the small-flow timescales]. In this situation, the final equations are rather simple (although the physics is of course complex) and fractional step methods become very efficient. However, with nonorthogonal meshes, which are required to simulate the confined flow around cylinders or spheres in a channel, for example, and with higher-order advection schemes, which introduce nonlinearities, iterations are necessary in order to achieve a stationary state.

Many authors have followed the fractional-step, noniterative approach to devise methods with second-order accuracy in time for viscoelastic flows, with applications mostly restricted to Cartesian coordinate meshes, as in the references above except for Richter et al. (2010), who dealt with the viscoelastic vortex shedding flow past a cylinder at moderate to high Re ($Re \sim 100-300$). More recently, it has been shown that fractional-step implicit-explicit methods (Ascher et al. 1995) are effective at solving viscoelastic problems with FEM even in nonorthogonal meshes (D'Avino & Hulsen 2010, D'Avino et al. 2012, Castillo & Codina 2015), with these authors dealing with typical viscoelastic test problems, such as creeping flow around cylinders and spheres. On the contrary, when iterative methods are preferred due to the more complex nature of the problems, or if fractional steps are applied with iteration due to implicit treatment of some nonlinear terms, it has been shown that significant improvements can be gained by a simple substitution of the dependent variables: For example, in FENE-P-like constitutive equations, if the stress ($\boldsymbol{\tau}_p$) is replaced by the reduced stress ($\boldsymbol{\tau}_p/f$), the number of iterations within a time step, in time-dependent problems, is reduced by one order of magnitude (Oliveira 2017). Conversely, the rate of convergence of iterative solution algorithms using the transformation suggested by Vaithianathan & Collins (2003), explained in Section 3.1.2.3, may be negatively affected by such a change of variables [since $\mathbf{A} \rightarrow \hat{\mathbf{A}} = f(\mathbf{A})\mathbf{A}$ is equivalent to $\boldsymbol{\tau}_p/f \rightarrow \boldsymbol{\tau}_p$].

3.3.3. Direct versus sequential methods. In simulations of viscoelastic flows with incompressible liquids, in addition to the classical velocity/pressure problem also present in standard CFD, which requires solving three momentum equations and one Poisson pressure or pressure-correction equation, one needs to solve six additional equations for determining the stress components (or the conformation tensor). These coupled equations prompt the question of whether it is desirable to solve the whole set, or parts of it, in a direct way, thus allowing the solution for $\mathbf{u}$ and $\boldsymbol{\tau}$ to be obtained simultaneously. While in the past, FEM studies in relatively coarse meshes were often based on such direct methods (e.g., Marchal & Crochet 1987, King et al. 1988), there is presently a tendency to apply the same procedures in the FVM context even for much finer meshes (Fernandes et al. 2019, Pimenta & Alves 2019).

An alternative approach, which appears to be more effective but has not been tested extensively, is to solve the velocity/pressure problem as in standard CFD, with the stress divergence term evaluated explicitly, and to treat the stress problem by iteration encompassing only the six constitutive equations. Experience shows that these equations are much faster to solve than the equation of motion, requiring only a few inner iterations of an iterative solver, such as BCG (biconjugate gradient) or GMRES (generalized minimal residual). Incidentally, numerical experiments conducted by Oliveira, but not published in Oliveira (2017), showed that only two outer iterations over the constitutive equations set were sufficient for the individual stress components to be evaluated consistently (similar to the direct solution of those equations, as in the grid-by-grid method mentioned in Section 3.1.1). Oliveira (2017) reported that the amplification factor for the reduced stress ($\boldsymbol{\tau}/f$) formulation with FENE-CR or FENE-P models is much smaller than for the actual

stress by a factor of $\Delta t/\lambda$, thus explaining the reduction in the number of global outer iterations within a time step Δt (to about three or four iterations). Recently, Pimenta & Alves (2019) showed that although coupled solvers are slower on a per-time-step basis, they can be made significantly faster using semicoupled solvers applied to electrically driven flows of viscoelastic fluids.

4. BENCHMARK FLOWS

Obtaining agreement between experiments and numerical simulations of viscoelastic fluid flows, even in simple canonical geometries, is not straightforward. The differences typically observed can be attributed either to numerical errors or to the inadequacy of the constitutive equation used to reproduce the fluid rheology. The latter issue is not easy to circumvent due to the limited availability of constitutive equations that can accurately reproduce the complex behavior of a viscoelastic fluid in all flows, not to mention for all fluids, as discussed in Section 2.

To better identify the origin of the errors induced by the numerical approximations and to allow a precise comparison between different flow solvers, researchers have proposed over the last few decades a limited set of geometrically simple reference flows. In CR, most benchmark flows have been proposed in the long-standing biannual International Workshops on Numerical Methods for Non-Newtonian Flows, which started in 1979. Early on, the focus was to understand why the numerical solutions would break down invariably at rather small values of *Wi* and to overcome this limitation: the well-known HWNP (Walters 1982). The earliest benchmark was the 4:1 sudden contraction flow, where the sharp corner in the flow domain creates a stress singularity (Hinch 1993) that is known to cause numerical instabilities. Therefore, at the third workshop, researchers introduced the smooth flow around a sphere as a new benchmark flow (Armstrong et al. 1984).

The fourth workshop, in 1985, included experimentalists in order to provide valuable data for comparison with numerical simulations (Crochet 1986). To separate elastic from shear rate–dependent viscosity effects, researchers based experiments and numerical simulations on the so-called Boger fluids (James 2009), a class of viscoelastic fluids that have a nearly shear rate–independent shear viscosity and that can be modeled approximately with the Oldroyd-B model. The accuracy of the numerical solutions was a critical issue at the time (and still is) because of the use of low-order schemes and coarse meshes, mainly due to hardware limitations. Spurious mesh-dependent solutions and instabilities were identified as a critical issue to overcome.

At those early times, the numerical simulations were based primarily on the FEM (Crochet & Walters 1983, Crochet et al. 1984, Owens & Phillips 2002), and besides the typical 4:1 contraction flow (planar and axisymmetric), other viscoelastic benchmark flows included the flow between eccentric rotating cylinders, flow past a translating sphere, cavity flows, and the two-phase extrudate swell flow. Differential and integral constitutive equations were used, and 3D and time-dependent flow calculations had already been reported. However, since the number of available simulation test cases was large, there was an agreement at the fifth workshop (1987) to focus primarily on the following set of benchmark problems (Leal et al. 1988): (*a*) steady motion of a sphere in a cylinder, with a ratio of 0.5 between the sphere and tube diameters (previously proposed in the third workshop); (*b*) flow in a tube with sinusoidal cross section; (*c*) eccentric rotating cylinder flow; (*d*) stick–slip flow in a channel; and (*e*) 4:1 planar and axisymmetric contraction flows.

The first three benchmarks refer to smooth flow problems, whereas the last two include singular geometrical points in the flow domain, such as the reentrant corners in a sudden contraction flow, where the velocity gradient, pressure, and extra stresses are unbounded, leading to increased numerical difficulty. In terms of constitutive equations, the UCM and Oldroyd-B models were the primary choices, aimed at representing Boger fluids. These constitutive equations are the most challenging numerically, making them an ideal choice to test the robustness and accuracy of new

numerical methods. However, quantitative agreement between experiments and numerical simulations is not guaranteed for such simple constitutive models.

Experimental difficulties in investigating the flow past a confined sphere with a 2:1 diameter ratio led to a change of the benchmark problems at the seventh workshop (Baird & Renardy 1992). Alternative, simpler flows of the same type were proposed, consisting of the flow past an unbounded sphere and the 2D flow past a confined cylinder (Brown & McKinley 1994).

This series of workshops has been important for the fruitful exchange of ideas and the development of stable and accurate methods for viscoelastic fluid flow simulations, several of which were presented in Section 3. The scope of the workshops has broadened over the years and covers topics not addressed in this review. Similarly, the benchmark problems have also evolved and currently there seems to be a predilection for the following test cases: (*a*) flow past a cylinder in a channel, with a ratio of 0.5 between the cylinder diameter and channel width (e.g., Knechtges et al. 2014, Carrozza et al. 2019); (*b*) 4:1 planar and axisymmetric contractions (e.g., Pimenta & Alves 2017, Niethammer et al. 2019); (*c*) flow in a lid-driven cavity (e.g., Fattal & Kupferman 2005, Fernandes et al. 2019, Syrakos et al. 2020); (*d*) flow in cross-slot devices (e.g., Cruz et al. 2014, Kalb et al. 2018, Zografos et al. 2018); and (*e*) die swell (e.g., Comminal et al. 2018, Spanjaards et al. 2019, Tang et al. 2019). The Oldroyd-B and UCM models continue to be frequent choices, but there is also a significant number of works dealing with other constitutive equations. Below we briefly describe three of these benchmark problems.

4.1. Flow in a Planar 4:1 Contraction

The geometry of this benchmark flow is illustrated in the inset of **Figure 1*b***. The fluid flows from left to right, and an abrupt reduction of the channel width, with a 4:1 ratio, occurs at the contraction plane, generating a complex flow field despite the simplicity of the geometry. In the centerline region the flow is extensionally dominated, while near the walls the flow is shear dominated, with an unbounded variation of the pressure and stress fields as the reentrant corners are approached. For Newtonian fluids, the flow field only depends on the Reynolds number, while for

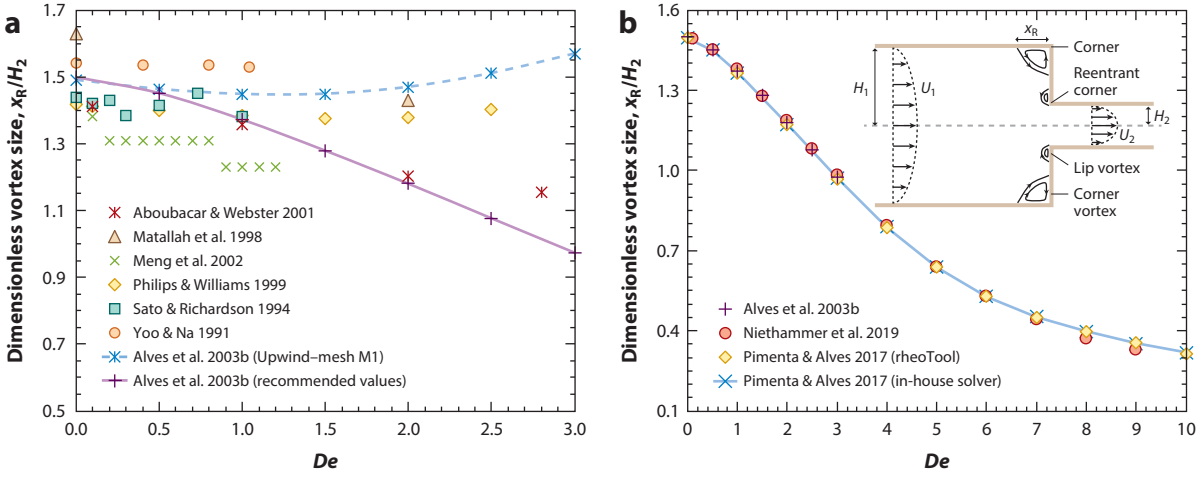

Figure 1

Dimensionless vortex size, x_R/H_2, as a function of Deborah number, *De*, for the 4:1 planar contraction flow of an Oldroyd-B fluid with a solvent viscosity ratio of $\beta = 1/9$ under creeping flow conditions. (*a*) Comparison between numerical results available in 2003 and (*b*) between recent works. Panel *a* adapted with permission from Alves et al. (2003b), copyright 2003 Elsevier.

viscoelastic fluids a new dimensionless parameter is required to characterize flow elasticity. The Deborah number is typically used for this purpose (in steady flow *Wi* can alternatively be used), here defined as $De = \lambda U_2/H_2$, where U_2 is the average velocity at the downstream (narrower) channel of half-width, H_2. Depending on the constitutive equation, additional dimensionless numbers might be required, which are specific to the model (or to the fluid in the experiments). For example, the Oldroyd-B model is frequently used in this test case, and the solvent viscosity ratio ($\beta = \eta_s/\eta_0$) is needed, with the value $\beta = 1/9$ typically used in most works.

Other planar contraction ratios have also been studied experimentally and numerically (e.g., Evans & Walters 1986, Alves et al. 2004), and the axisymmetric geometry has also been investigated in several works (e.g., McKinley et al. 1991, Nigen & Walters 2002, Oliveira et al. 2007, López-Aguilar et al. 2016).

An overview of numerical data until 2003 was presented by Alves et al. (2003b), here adapted as **Figure 1*a***. Despite the effort put to this problem by several research groups for more than three decades, it was frustrating to realize that no agreement could be found among the available numerical data in 2003, especially in the Newtonian limit. Alves et al. (2003b) presented a detailed study including the Oldroyd-B and PTT models and provided benchmark data in the steady-state regime. Surprisingly, it took one decade to corroborate these benchmark results (Omowunmi & Yuan 2013), and subsequent works have also found agreement in the steady-flow regime (Castillo & Codina 2014, Mirzakhalili & Nejat 2015, Comminal et al. 2016). Later, Pimenta & Alves (2017), using the log-conformation technique implemented in an open-source solver, presented accurate results up to $De = 12$, therefore including the steady- and unsteady-flow regimes. These results were independently confirmed by Niethammer et al. (2019) (cf. **Figure 1*b***), finally showing that this very stringent test case has benchmark data available to assess the accuracy of new solvers. To achieve such high *De*, both Pimenta & Alves (2017) and Niethammer et al. (2019) required the use of stabilization methods, and the log-conformation formulation of the constitutive equation seems to be a key aspect of the numerical stability. Afonso et al. (2011) showed that it was possible to simulate flows up to $De = 100$, even though the accuracy at such elasticity levels is questionable and the complexity of the flow patterns is not compatible with a 2D flow approximation. However, the use of the log-conformation approach has clearly opened up the possibility of simulating flows at very large *Wi*, allowing conditions typical of microfluidic viscoelastic flows to be simulated, namely high *Wi* and low *Re*. To this end, 3D meshes are mandatory, opening the possibility of reproducing and exploring in detail the elastic turbulence regime, which will require large computational times unless massively parallel computations are used.

4.2. Flow Past a Cylinder in a Planar Channel

This benchmark problem was proposed nearly three decades ago (Baird & Renardy 1992) and many numerical studies have been published since, mainly using the Oldroyd-B model under creeping flow conditions, with a solvent viscosity ratio of $\beta = 0.59$ (e.g., Fan et al. 1999, Alves et al. 2001, Owens et al. 2002, Hulsen et al. 2005, Coronado et al. 2007, Afonso et al. 2009, Damanik et al. 2010, Claus & Phillips 2013, Knechtges et al. 2014, Carrozza et al. 2019). The excellent agreement between the numerical data of Fan et al. (1999) and Alves et al. (2001) in the steady-flow regime, up to $De \approx 0.8$ (defined with the average velocity in the channel U and cylinder radius R), has been confirmed in several subsequent works, as illustrated in **Figure 2*a*** for the dimensionless drag force over the cylinder. This benchmark is arguably the most frequently used currently to assess the stability and accuracy of new numerical methods in CR. This choice is mainly due to the simplicity of the problem, combined with the availability of accurate benchmark data and the absence of singular points in the flow domain, at least in the low-*De* range (Bajaj et al. 2008).

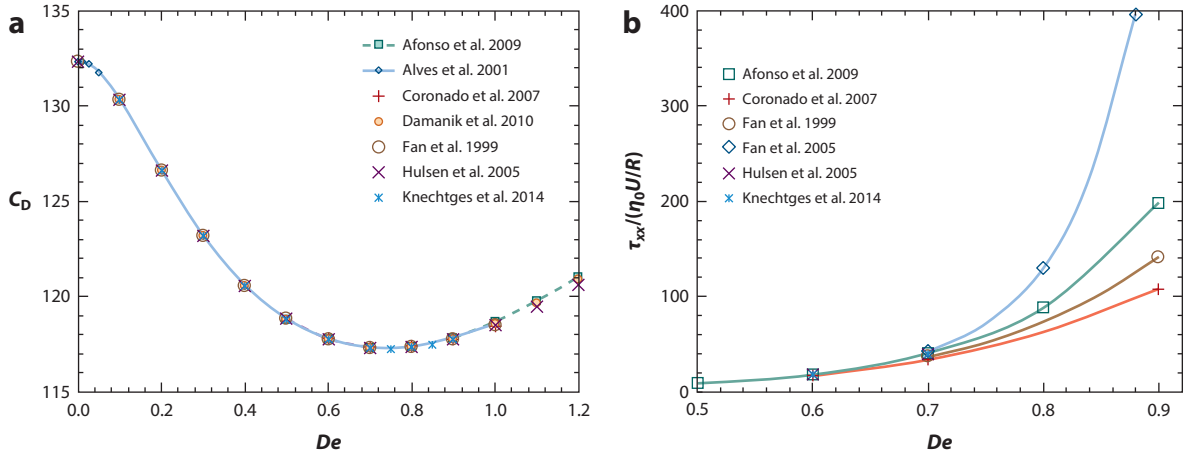

Figure 2

Comparison between different numerical results for the flow past a cylinder in a channel. (*a*) Drag force coefficient, C_D, as a function of Deborah number, $De = \lambda U/R$. (*b*) Maximum dimensionless normal stress, $\tau_{xx}/(\eta_0 U/R)$, along the cylinder wake centerline as a function of *De*. The curves are a guide to the eye.

Despite the progress made in this reference problem, the main challenges that remain to be addressed are (*a*) to determine accurately the critical *De* for transition from steady to time-dependent flow conditions; (*b*) to simulate accurately the stress fields in the cylinder wake, where very large stress gradients are observed approaching an unbounded behavior around $De \approx 0.7$ (Bajaj et al. 2008); and (*c*) to simulate accurately the unsteady-flow regime and reproduce the complex behavior observed in the experiments at very large *De* (Kenney et al. 2013), which will require the use of 3D meshes.

Figure 2*b* presents maximum values of the streamwise normal stress (τ_{xx}) along the downstream centerline, showing that the discrepancies among the available data are still significant. The differences observed between different methods increase sharply with *De*, as shown by Afonso et al. (2009). Since the numerical results are very sensitive to the accuracy of the methods used, this problem is ideal to assess convergence with mesh refinement and the order of convergence of numerical methods. Additionally, 3D simulations and experimental work for the corresponding flow about a confined cylinder were conducted by Ribeiro et al. (2014) and Varchanis et al. (2019a).

4.3. Flow in a Planar Cross-Slot Device

The cross-slot geometry is illustrated in **Figure 3** and consists of four orthogonal channels with opposite inlets and outlets in a symmetric configuration. In the central square region, the flow is extensionally dominated. In the vicinity of the central stagnation point, a birefringence strand develops along the centerline in the downstream direction, which can be used experimentally to measure the normal stresses and estimate the extensional viscosity of complex fluids (Coventry & Mackley 2008, Haward et al. 2012). Arratia et al. (2006) showed that viscoelastic fluids can undergo a series of flow transitions under creeping flow conditions: Newtonian-like flow patterns are observed at low *De*, followed by an intermediate steady-flow asymmetry, and finally a transition to unsteady flow at higher *De*, eventually achieving the elastic turbulence regime at very large *De* (Sousa et al. 2018). The steady-flow asymmetry is particularly interesting, and unexpected, but

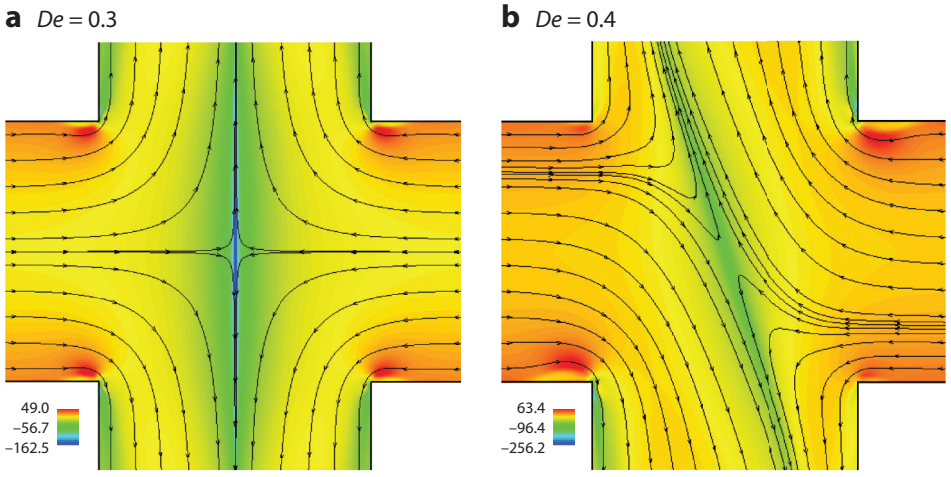

Figure 3

Streamline patterns and contour plots of normalized first normal stress difference, $N_1/(\eta U/D)$, where D is the channel width and U is the average velocity in each channel, using the upper-convected Maxwell model under creeping flow conditions with a Deborah number ($\lambda U/D$) of (*a*) $De = 0.3$ and (*b*) $De = 0.4$. Figure reprinted with permission from Poole et al. (2007), copyright 2007 American Physical Society.

only occurs for some fluids and over a narrow range of flow conditions (Sousa et al. 2015), hence its elusiveness. This steady-flow instability was experimentally documented in detail by Arratia et al. (2006) and soon after was qualitatively predicted numerically by Poole et al. (2007) using the UCM model. Besides this interesting flow transition, this flow field develops unbounded stresses at the stagnation point for UCM and Oldroyd-B models when the local strain rate $\dot{\varepsilon}$ exceeds $1/(2\lambda)$, such that $Wi = \lambda\dot{\varepsilon} \geq 0.5$. Therefore, this flow problem can be used to assess the accuracy of numerical methods in a very stringent test with very large, or even unbounded, stress gradients developing in a region/point inside the flow domain, away from the boundaries.

This type of flow has relevant applications in extensional rheology, and the complex flow instabilities that are generated in such simple configuration are also interesting from a fundamental point of view. Cruz et al. (2014) provided detailed benchmark data for creeping flow conditions over a wide range of *De*, using several constitutive equations, including the UCM, Oldroyd-B, and PTT models in the steady symmetric and asymmetric regimes, both of which are illustrated in **Figure 3** for the UCM model.

The benchmark problems described clearly show that important progress has been made over the years, and currently for all of these 2D flows, data with good accuracy are available in the steady-flow regime. For transient computations, the lid-driven cavity benchmark has seen some recent progress, with several works presenting accurate data in the transient and steady-state regimes (e.g., Fattal & Kupferman 2005, Sousa et al. 2016, Syrakos et al. 2020). In the future, we suggest that the focus should lean toward 3D flows at very large *Wi* to improve our understanding of the elastic turbulence regime. The development of stabilizing techniques such as the log-conformation and square-root transformations has allowed researchers to finally surpass the longstanding HWNP, but the accuracy at large *De* is still a challenge due to the stringent requirements in terms of mesh refinement levels and the associated required computational resources. The proliferation of open-source codes, such as the viscoelasticFluidFoam (Favero et al. 2010) and the rheoTool libraries (Pimenta & Alves 2016) for OpenFOAM® or the Basilisk flow solver (Popinet 2020), is expected to increase the awareness and use of computational methods for

viscoelastic fluids. These open-source projects can also benefit from the collective improvement and implementation of new methods in a cooperative approach, ultimately advancing more rapidly their use and capabilities.

5. CURRENT DIRECTIONS

Viscoelastic flow simulation tools exist for the purpose of applications, which drive the development of numerical methods. While presenting these in Section 3, we have identified issues in need of further investigation. These issues are typically assessed in benchmark flows, such as those described in Section 4, where specific challenges have also been singled out. In this section, we briefly present some current and future needs. Space limitations do not allow for an extensive discussion, and certainly the interested reader will be able to identify additional worthy candidates.

5.1. Mesoscopic Models for Complex Fluids

This review concerns methods for continuum-level models, but as implied in Section 2, viscoelastic fluids involve interactions among macromolecules or particles. The full extent of the ensuing large number of degrees of freedom and wide spectrum of timescales is missed or inadequately described by the continuum-level models. Molecular dynamics is still too expensive, but those interactions can be captured with coarse-grained models of local fluid structures, relying on kinetic theory principles, which are followed in space and time to locally compute the stress field needed by the continuum-level momentum equation. These so-called micro-macro/mesoscopic approaches follow typically one of two methods: (*a*) The first method deals with the Fokker–Planck equation governing the distribution function of the coarse-grained configurations, used to compute the continuum-level polymer stress, and (*b*) the second is the stochastic approach, which benefits from the equivalence between the Fokker–Planck equation and Itô's stochastic differential equation for the configuration. An overview of both methods has been given by Keunings (2004). One of the stochastic techniques is the CONNFFESSIT (calculation of non-Newtonian flows: finite elements and stochastic simulation technique) method of Öttinger & Laso (1992), subject to improvements to address shortcomings, like the Brownian configuration fields of Hulsen et al. (1997) or the Lagrangian particle method of Halin et al. (1998).

Other mesoscopic methods have been under development, such as lattice Boltzmann (LB), smoothed particle hydrodynamics (SPH), and dissipative particle dynamics (DPD) [or smoothed DPD (SDPD)]. These methods are less expensive than the above stochastic techniques but are still in their infancy with respect to viscoelastic fluids. For LB with viscoelastic fluids, a good starting point is the works of Malaspinas et al. (2010) and Su et al. (2013). SPH, DPD, and SDPD are related to each other. For SPH, readers are referred to Ellero et al. (2002) and Ellero & Español (2018). For DPD, we suggest Español & Warren (2017) and the first extension to viscoelastic fluids by ten Bosch (1999). For SDPD with viscoelastic fluids, Vázquez-Quesada et al. (2012) and Litvinov et al. (2016) are important references.

5.2. Microfluidics

Inexpensive manufacturing of microfluidic circuits has opened up a wealth of applications. On account of their small length scales, *Re* is low and *Wi* can be high on such circuits, driving the fluid dynamics to new phenomena, including elastic turbulence (Groisman & Steinberg 2000) and other elasticity-driven flow transitions. The full range of phenomena in microscale flows of complex fluids needs to be further explored, and some of the challenges involve the combination

of viscoelasticity with electrokinetics (e.g., electro-elastic instabilities, as investigated by Afonso et al. 2012b) or with other relevant forcing methods. Gas–liquid and especially liquid–liquid flows are also common in microfluidics (Anna 2016).

5.3. Multiphase Flows

Multiphase flows are industrially relevant in a wide range of applications and require specific numerical methods (e.g., Sommerfeld 2017). The use of complex fluids in one or both liquid phases is quite relevant for applications in microfluidics, and here the volume-of-fluid (VOF) and level set methods are often used (see Habla et al. 2011 for numerical developments of VOF). Suspensions in viscoelastic liquids are also relevant, and the topic was recently reviewed by D'Avino & Maffettone (2015).

The marker-and-cell method has been used, for example, in the droplet-splashing simulations of Palhares et al. (2016). The same flow problem has also been recently investigated by López-Herrera et al. (2019), who used VOF together with the adaptive meshing technique in the Basilisk flow solver of Popinet (2020) for a more accurate description of the large gradients near the interface, combined with an established time-split scheme to improve the stability of the two-phase flow. Regardless of the combination of fluid phases, the accurate and efficient description of the dynamics of the viscoelastic fluid requires the combination of the interface method with one of the techniques described above to deal adequately with viscoelastic fluids, such as the log-conformation or the square-root-conformation techniques.

Numerical difficulties still exist related with the interfacial force discretization and in some problems when the two fluid phases have order-of-magnitude differences in viscosity and density.

5.4. Turbulent Flows

The addition of small amounts of polymer molecules or surfactants in otherwise Newtonian fluids has a large impact on the turbulence dynamics in inertia-driven wall turbulence, leading to drag reductions that can exceed 80%. Major progress has taken place over the last 25 years, especially due to numerical investigations of fully developed channel flow via DNS (Sureshkumar et al. 1997, Vaithianathan et al. 2006), and only in more recent years has research turned to other canonical flows like homogeneous turbulence (Valente et al. 2014) or shear-driven wall-free turbulence (Vaithianathan et al. 2007). Numerical methods and stabilization techniques for viscoelastic fluids have advanced significantly to allow for such complex computations, and the time is right to extend fundamental investigations to other turbulent canonical flows in order to understand the physics of their turbulence and to develop turbulence models based on Reynolds-averaged Navier–Stokes equations (Masoudian et al. 2015) and LES (Ferreira et al. 2016).

5.5. Flows of Thixotropic Elasto-Visco-Plastic Materials

By adding more than just polymer molecules to Newtonian solvents, and not necessarily in small fractions, a wide range of engineered fluids and materials is obtained, which combine in various degrees several complex material properties. The thixotropic elasto-visco-plastic (TEVP) material is a good example of the complexity of the challenges involved. The rheological modeling is very challenging, as recently shown by Varchanis et al. (2019b). From a numerical point of view, besides the difficulties associated with viscoelasticity, there are also the effects of yield stress; in particular, one needs to efficiently and accurately follow the interface between yielded (fluid) and nonyielded material. Saramito & Wachs (2017) presented a recent review of numerical methods for yield

stress materials. Multiphase flows of TEVP materials add to the numerical challenge and remain uncharted territory.

DISCLOSURE STATEMENT

The authors are not aware of any biases that might be perceived as affecting the objectivity of this review.

ACKNOWLEDGMENTS

The authors are indebted to the contributions of former students and colleagues with whom they have interacted extensively on numerical methods and applications for viscoelastic fluids. In particular, we would like to acknowledge lengthy discussions and work over the last 20 years with Drs. Alexandre Afonso, Filipe Cruz, Miguel Nóbrega, Cássio Oishi, Mónica Oliveira, and Murilo Tomé; Mr. Francisco Pimenta; and Profs. Marcel Escudier, Gareth McKinley, Robert Poole, Carlos B. Silva, Radhakrishna Sureshkumar, and Bassam Younis. In addition, F.T.P. and M.A.A. acknowledge funding from Fundação para a Ciência e a Tecnologia (FCT) via projects UIDB/00532/2020 and UIDP/00532/2020, and P.J.O. is grateful to FCT project UIDB/00151/2020 and to project EMaDes (Centro-01-0145-FEDER-17).

LITERATURE CITED

Aboubacar M, Webster MF. 2001. A cell-vertex finite volume/element method on triangles for abrupt contraction viscoelastic flows. *J. Non-Newton. Fluid Mech.* 98:83–106

Afonso AM, Oliveira MSN, Oliveira PJ, Alves MA, Pinho FT. 2012a. The finite volume method in computational rheology. In *Finite Volume Method: Powerful Means of Engineering Design*, ed. R Petrova, pp. 141–70. London: InTech Open

Afonso AM, Oliveira PJ, Pinho FT, Alves MA. 2009. The log-conformation tensor approach in the finite volume method framework. *J. Non-Newton. Fluid Mech.* 157:55–65

Afonso AM, Oliveira PJ, Pinho FT, Alves MA. 2011. Dynamics of high-Deborah-number entry flows: a numerical study. *J. Fluid Mech.* 677:272–304

Afonso AM, Pinho FT, Alves MA. 2012b. Electro-osmosis of viscoelastic fluids and prediction of electro-elastic instabilities in a cross slot using a finite volume method. *J. Non-Newton. Fluid Mech.* 179–180:55–68

Afonso AM, Pinho FT, Alves MA. 2012c. The *kernel-conformation* constitutive laws. *J. Non-Newton. Fluid Mech.* 167–168:30–37

Alves MA, Oliveira PJ, Pinho FT. 2003a. A convergent and universally bounded interpolation scheme for the treatment of advection. *Int. J. Numer. Methods Fluids* 41:47–75

Alves MA, Oliveira PJ, Pinho FT. 2003b. Benchmark solutions for the flow of Oldroyd-B and PTT fluids in planar contractions. *J. Non-Newton. Fluid Mech.* 110:45–75

Alves MA, Oliveira PJ, Pinho FT. 2004. On the effect of contraction ratio in viscoelastic flow through abrupt contractions. *J. Non-Newton. Fluid Mech.* 122:117–30

Alves MA, Pinho FT, Oliveira PJ. 2000. Effect of a high-resolution differencing scheme on finite-volume predictions of viscoelastic flows. *J. Non-Newton. Fluid Mech.* 93:287–314

Alves MA, Pinho FT, Oliveira PJ. 2001. The flow of viscoelastic fluids past a cylinder: finite-volume high-resolution methods. *J. Non-Newton. Fluid Mech.* 97:207–232

Amoreira LJ, Oliveira PJ. 2010. Comparison of different formulations for the numerical calculation of unsteady incompressible viscoelastic fluid flow. *Adv. Appl. Math. Mech.* 2:483–502

Anna SL. 2016. Droplets and bubbles in microfluidic devices. *Annu. Rev. Fluid Mech.* 48: 285–309

Armstrong RC, Brown RA, Caswell B. 1984. Papers from the Third International Workshop on Numerical Simulation of Viscoelastic Flows. *J. Non-Newton. Fluid Mech.* 16:1–2

Arratia PE, Thomas CC, Diorio J, Gollub JP. 2006. Elastic instabilities of polymer solutions in cross-channel flow. *Phys. Rev. Lett.* 96:144502

Ascher UM, Ruuth SJ, Wetton BTR. 1995. Implicit-explicit methods for time-dependent partial differential equations. *SIAM J. Numer. Anal.* 32:797–823
Baaijens FPT. 1998. Mixed finite element methods for viscoelastic flow analysis: a review. *J. Non-Newton. Fluid Mech.* 79:361–285
Balci N, Thomases B, Renardy M, Doering CR. 2011. Symmetric factorization of the conformation tensor in viscoelastic fluid models. *J. Non-Newton. Fluid Mech.* 166:546–53
Baird DG, Renardy M. 1992. Report on the VIIth International Workshop on Numerical Methods in Non-Newtonian Flow. *J. Non-Newton. Fluid Mech.* 43:383–85
Bajaj M, Pasquali M, Prakash JR. 2008. Coil-stretch transition and the breakdown of computations for viscoelastic fluid flow around a confined cylinder. *J. Rheol.* 52:197–223
Bird RB, Armstrong RC, Hassager O. 1987a. *Dynamics of Polymeric Liquids*, Vol. 1: *Fluid Mechanics*. New York: Wiley. 2nd ed.
Bird RB, Curtiss CF, Armstrong RC, Hassager O. 1987b. *Dynamics of Polymeric Liquids*. Vol. 2: *Kinetic Theory*. New York: Wiley. 2nd ed.
Bird RB, Dotson PJ, Johnson NL. 1980. Polymer solution rheology based on a finitely extensible bead-spring chain model. *J. Non-Newton. Fluid Mech.* 7:213–35
Bird RB, Wiest JM. 1995. Constitutive equations for polymeric liquids. *Annu. Rev. Fluid Mech.* 27:169–93
Brown RA, McKinley GH. 1994. Report on the VIIIth International Workshop on Numerical Methods in Viscoelastic Flows. *J. Non-Newton. Fluid Mech.* 52:407–13
Carrozza MA, Hulsen MA, Hütter M, Anderson PD. 2019. Viscoelastic fluid flow simulation using the contravariant deformation formulation. *J. Non-Newton. Fluid Mech.* 270:23–35
Castillo E, Codina R. 2014. Variational multi-scale stabilized formulations for the stationary three-field incompressible viscoelastic flow problem. *Comput. Meth. Appl. Mech. Eng.* 279:579–605
Castillo E, Codina R. 2015. First, second and third order fractional step methods for the three-field viscoelastic flow problem. *J. Comput. Phy.* 296:113–37
Chilcott DM, Rallison JM. 1988. Creeping flow of dilute polymer solutions past cylinders and spheres. *J. Non-Newton. Fluid Mech.* 29:381–432
Chorin AJ. 1968. Numerical solution of the Navier-Stokes. *Math. Comput.* 22:745–62
Claus S, Phillips TN. 2013. Viscoelastic flow around a confined cylinder using spectral/hp element methods. *J. Non-Newton. Fluid Mech.* 200:131–46
Comminal R, Hattel JH, Alves MA, Spangenberg J. 2016. Vortex behavior of the Oldroyd-B fluid in the 4-1 planar contraction simulated with the streamfunction–log-conformation formulation. *J. Non-Newton. Fluid Mech.* 237:1–15
Comminal R, Pimenta F, Hattel JH, Alves MA, Spangenberg J. 2018. Numerical simulation of the planar extrudate swell of pseudoplastic and viscoelastic fluids with the streamfunction and the VOF methods. *J. Non-Newton. Fluid Mech.* 252:1–18
Coronado O, Arora D, Behr M, Pasquali M. 2007. A simple method for simulating general viscoelastic fluid flows with an alternate log-conformation formulation. *J. Non-Newton. Fluid Mech.* 147:189–99
Coventry KD, Mackley MR. 2008. Cross-slot extensional flow birefringence observations of polymer melts using a multi-pass rheometer. *J. Rheol.* 52:401–15
Crochet M. 1986. Foreword to the Proceedings of the Fourth Workshop on Numerical Methods in Viscoelastic Flow. *J. Non-Newton. Fluid Mech.* 20:1–9
Crochet MJ, Davies AR, Walters K. 1984. *Numerical Simulation on Non-Newtonian Flow*. Amsterdam: Elsevier
Crochet MJ, Walters K. 1983. Numerical methods in non-Newtonian fluid mechanics. *Annu. Rev. Fluid Mech.* 15:241–60
Cruz FA, Poole RJ, Afonso AM, Pinho FT, Oliveira PJ, Alves MA. 2014. A new viscoelastic benchmark flow: stationary bifurcation in a cross-slot. *J. Non-Newton. Fluid Mech.* 214:57–68
Damanik H, Hron J, Ouazzi A, Turek S. 2010. A monolithic FEM approach for the log-conformation reformulation (LCR) of viscoelastic flow problems. *J. Non-Newton. Fluid Mech.* 165:1105–13
Darwish MS, Whiteman JR, Bevis MJ. 1992. Numerical modelling of viscoelastic liquids using a finite volume method. *J. Non-Newton. Fluid Mech.* 45:311–37
D'Avino G, Hulsen MA. 2010. Decoupled second-order transient schemes for the flow of viscoelastic fluids without a viscous solvent contribution. *J. Non-Newton. Fluid Mech.* 165:1602–12

D'Avino G, Hulsen MA, Maffettone PL. 2012. Decoupled transient schemes for viscoelastic fluid flow with inertia. *Comput. Fluids* 66:183–93

D'Avino G, Maffettone PL. 2015. Particle dynamics in viscoelastic liquids. *J. Non-Newton. Fluid Mech.* 215:80–104

Duarte ASR, Miranda AIP, Oliveira PJ. 2008. Numerical and analytical modeling of unsteady viscoelastic flows: the start-up and pulsating test case problems. *J. Non-Newton. Fluid Mech.* 154:153–69

Dubief Y, Terrapon VE, White CM, Shaqfeh ESG, Moin P, Lele SK. 2005. New advances on the interaction between polymers and vortices in turbulent flows. *Flow Turb. Comb.* 74:311–29

Dupret F, Marchal JM. 1986. Sur le signe des valeurs propres du tenseur des extra-constraints dans un écoulement de fluide de Maxwell. *J. Méc. Théor. Appl.* 5:403–27

Edussuriya SS, Williams AJ, Bailey C. 2004. A cell-centred finite volume method for modelling viscoelastic flow. *J. Non-Newton. Fluid Mech.* 117:47–61

El-Kareh AW, Leal GL. 1989. Existence of solutions for all Deborah numbers for a non-Newtonian model modified to include diffusion. *J. Non-Newton. Fluid Mech.* 33:257–87

Ellero M, Español P. 2018. Everything you always wanted to know about SDPD (but were afraid to ask). *Appl. Math. Mech.* 39:103–24

Ellero M, Kröger M, Hess S. 2002. Viscoelastic flows studied by smoothed particle dynamics. *J. Non-Newton. Fluid Mech.* 105:35–51

Español P, Warren P. 2017. Perspective: dissipative particle dynamics. *J. Chem. Phys.* 146:150901

Evans JD, Oishi CM. 2017. Transient computations using the natural stress formulation for solving sharp corner flows. *J. Non-Newton. Fluid Mech.* 249:48–52

Evans RE, Walters K. 1986. Flow characteristics associated with abrupt changes in geometry in the case of highly elastic liquids. *J. Non-Newton. Fluid Mech.* 20:11–29

Fan Y, Tanner R, Phan-Thien N. 1999. Galerkin/least-square finite-element methods for steady viscoelastic flows. *J. Non-Newton. Fluid Mech.* 84:233–56

Fan Y, Yang H, Tanner RI. 2005. Stress boundary layers in the viscoelastic flow past a cylinder in a channel: limiting solutions. *Acta Mech. Sin.* 21:311–21

Fattal R, Kupferman R. 2004. Constitutive laws for the matrix-logarithm of the conformation tensor. *J. Non-Newton. Fluid Mech.* 123:281–85

Fattal R, Kupferman R. 2005. Time-dependent simulation of viscoelastic flows at high Weissenberg number using the log-conformation representation. *J. Non-Newton. Fluid Mech.* 126:23–37

Favero J, Secchi A, Cardozo N, Jasak H. 2010. Viscoelastic fluid analysis in internal and in free surface flows using the software OpenFoam. *Comput. Chem. Eng.* 34:1984–93

Fernandes C, Vukčević V, Uroić T, Simões R, Carneiro OS, et al. 2019. A coupled finite volume flow solver for the solution of incompressible viscoelastic flows. *J. Non-Newton. Fluid Mech.* 265:99–115

Ferreira PO, Pinho FT, da Silva CB. 2016. Large-eddy simulations of forced isotropic turbulence with viscoelastic fluids described by the FENE-P model. *Phys. Fluids* 28:125104

Ferziger JH, Perić M. 2002. *Computational Methods for Fluid Dynamics*. Berlin: Springer-Verlag. 3rd ed.

Fiétier N, Deville MO. 2003. Time-dependent algorithms for the simulation of viscoelastic flows with spectral element methods: applications and stability. *J. Comput. Phys.* 186:93–121

Gaskell PH, Lau AKC. 1988. Curvature compensated convective transport: SMART, a new boundedness preserving transport algorithm. *Int. J. Numer. Methods Fluids* 8:617–41

Giesekus H. 1982. A simple constitutive equation for polymer fluids based on the concept of deformation-dependent tensorial mobility. *J. Non-Newton. Fluid Mech.* 11:69–109

Groisman A, Steinberg V. 2000. Elastic turbulence in a polymer solution flow. *Nature* 405:53–55

Guénette R, Fortin M. 1995. A new mixed finite element method for computing viscoelastic flows. *J. Non-Newton. Fluid Mech.* 60:27–52

Gupta A, Vincenzi D. 2018. Effect of polymer stress diffusion in the numerical simulation of elastic turbulence. *J. Fluid Mech.* 870:405–18

Habla F, Marschall H, Hinrichsen O, Dietsche L, Jasak H, Favero JL. 2011. Numerical simulation of viscoelastic two-phase flows using openFOAM. *Chem. Eng. Sci.* 66:5487–96

Habla F, Woitalka A, Neuner S, Hinrichsen O. 2012. Development of a methodology for numerical simulation of non-isothermal viscoelastic fluid flows with application to axisymmetric 4:1 contraction flows. *Chem. Eng. J.* 207–208: 772–84
Halin P, Lielens G, Keunings R, Legat V. 1998. The Lagrangian particle method for macroscopic and micro-macro viscoelastic flow computations. *J. Non-Newton. Fluid Mech.* 79:387–403
Haward SJ, Oliveira MSN, Alves MA, McKinley GH. 2012. Optimized cross-slot flow geometry for microfluidic extensional rheometry. *Phys. Rev. Lett.* 109:128301
Hinch MA. 1993. The flow of an Oldroyd fluid around a sharp corner. *J. Non-Newton. Fluid Mech.* 50:161–71
Housiadas KD, Beris AN. 2003. Polymer-induced drag reduction: effects of the variations in elasticity and inertia in turbulent viscoelastic channel flow. *Phys. Fluids* 15:2369–84
Housiadas KD, Wang L, Beris AN. 2010. A new method preserving the positive definiteness of a second order tensor variable in flow simulations with application to viscoelastic turbulence. *Comput. Fluids* 39:225–41
Hulsen MA. 1990. A sufficient condition for a positive definite configuration tensor in differential models. *J. Non-Newton. Fluid Mech.* 38:93–100
Hulsen MA, Fattal R, Kupferman R. 2005. Flow of viscoelastic fluids past a cylinder at high Weissenberg number: stabilized simulations using matrix logarithms. *J. Non-Newton. Fluid Mech.* 127:27–39
Hulsen MA, van Heel APG, van den Brule BHAA. 1997. Simulation of viscoelastic flows using Brownian configuration fields. *J. Non-Newton. Fluid Mech.* 70:79–101
James DF. 2009. Boger fluids. *Annu. Rev. Fluid Mech.* 41:129–42
Joseph DD. 1990. *Fluid Dynamics of Viscoelastic Liquids*. Berlin: Springer-Verlag
Kalb A, Villasmil-Urdaneta LA, Cromer M. 2018. Elastic instability and secondary flow in cross-slot flow of wormlike micellar solutions. *J. Non-Newton. Fluid Mech.* 262:79–91
Kenney S, Poper K, Chapagain G, Christopher GF. 2013. Large Deborah number flows around confined microfluidic cylinders. *Rheol. Acta* 52:485–97
Keshtiban IJ, Belblidia F, Webster MF. 2004. Numerical simulation of compressible viscoelastic liquids. *J. Non-Newton. Fluid Mech.* 122:131–46
Keunings R. 2003. Finite element methods for integral viscoelastic fluids. *Rheol. Rev.* 1:167–95
Keunings R. 2004. Micro-macro methods for the multi-scale simulation of viscoelastc flow using molecular models of kinetic theory. *Rheol. Rev.* 2:67–98
Kim J, Moin P. 1985. Application of a fractional-step method to incompressible Navier-Stokes equations. *J. Comput. Phys.* 59:308–23
King RC, Apelian MR, Armstrong RC, Brown RA. 1988. Numerically stable finite element techniques for viscoelastic calculations in smooth and singular geometries. *J. Non-Newton. Fluid Mech.* 29:147–216
Knechtges P, Behr M, Elgeti M. 2014. Fully-implicit log-conformation formulation of constitutive laws. *J. Non-Newton. Fluid Mech.* 214:78–87
Kurganov A, Tadmor E. 2000. New high-resolution central schemes for nonlinear conservation laws and convection-diffusion equations. *J. Comput. Phys.* 160:241–82
Larson RG. 1988. *Constitutive Equations for Polymer Melts and Solutions*. Stoneham, MA: Butterworth
Larson RG, Desai PS. 2015. Modeling the rheology of polymer melts and solutions. *Annu. Rev. Fluid Mech.* 47:47–65
Leal LG, Denn MM, Keunings R. 1988. Lake Arrowhead Workshop special issue papers—introduction. *J. Non-Newton. Fluid Mech.* 29:1–8
Likhtman AE, Graham RS. 2003. Simple constitutive equation for linear polymer melts derived from molecular theory: Rolie-Poly equation. *J. Non-Newton. Fluid Mech.* 114:1–12
Litvinov S, Xie QG, Hu XY, Adams NA, Ellero M. 2016. Simulation of individual polymer chains and polymer solutions with smoothed dissipative particle dynamics. *Fluids* 1:7
López-Aguilar JE, Tamaddon-Jahromi HR, Webster MF, Walters K. 2016. Numerical versus experimental pressure drops for Boger fluids in sharp-corner contraction flow. *Phys. Fluids* 28:103104
López-Herrera JM, Popinet S, Castrejón-Pita AA. 2019. An adaptive solver for viscoelastic incompressible two-phase problems applied to the study of the splashing of weakly viscoelastic droplets. *J. Non-Newton. Fluid Mech.* 264:144–58
Lozinski A, Owens RG. 2003. An energy estimate for the Oldroyd-B model: theory and applications. *J. Non-Newton. Fluid Mech.* 112:161–76

Malaspinas O, Fiétier N, Deville M. 2010. Lattice Boltzmann method for the simulation of viscoelastic fluid flows. *J. Non-Newton. Fluid Mech.* 165:1637–53

Marchal JM, Crochet MJ. 1987. A new mixed finite element for calculating viscoelastic flow. *J. Non-Newton. Fluid Mech.* 26:77–114

Masoudian M, Kim K, Pinho FT, Sureshkumar R. 2015. A Reynolds stress model for turbulent flow of homogeneous polymer solutions. *Int. J. Heat Fluid Flow* 54:220–35

Matallah H, Townsend P, Webster MF. 1998. Recovery and stress-splitting schemes for viscoelastic flows. *J. Non-Newton. Fluid Mech.* 75:139–66

McKinley GH, Raiford WP, Brown RA, Armstrong RC. 1991. Nonlinear dynamics of viscoelastic flow in axisymmetric abrupt contractions. *J. Fluid Mech.* 223:411–56

McLeish TCB, Larson RG. 1998. Molecular constitutive equations for a class of branched polymers: the pom-pom polymer. *J. Rheol.* 42:81–110

Meng S, Li XK, Evans G. 2002. Numerical simulation of Oldroyd-B fluid in a contraction channel. *J. Supercomput.* 22:29–43

Mirzakhalili E, Nejat A. 2015. High-order solution of viscoelastic fluids using the discontinuous Galerkin method. *J. Fluids Eng.* 137:031205

Mompean G, Deville M. 1997. Unsteady finite volume simulations of Oldroyd-B fluid through a three-dimensional planar contraction. *J. Non-Newton. Fluid Mech.* 72:253–79

Niethammer M, Marschall H, Kunkelmann C, Bothe D. 2018. A numerical stabilization framework for viscoelastic fluid flow using the finite volume method on general unstructured meshes. *Int. J. Numer. Methods Fluids* 86:131–66

Niethammer M, Marschall H, Bothe D. 2019. Robust direct numerical simulation of viscoelastic flows. *Chem. Ing. Tech.* 91:522–28

Nigen S, Walters K. 2002. Viscoelastic contraction flows: comparison of axisymmetric and planar configurations. *J. Non-Newton. Fluid Mech.* 102:343–59

Oldroyd JG. 1950. On the formulation of rheological equations of state. *Proc. R. Soc. A* 200:523–41

Oliveira MSN, Oliveira PJ, Pinho FT, Alves MA. 2007. Effect of contraction ratio upon viscoelastic flow in contractions: the axisymmetric case. *J. Non-Newton. Fluid Mech.* 147:92–108

Oliveira PJ. 2000. A traceless stress tensor formulation for viscoelastic fluid flow. *J. Non-Newton. Fluid Mech.* 95:55–65

Oliveira PJ. 2001. Method for time-dependent simulations of viscoelastic flows: vortex shedding behind cylinder. *J. Non-Newton. Fluid Mech.* 101:113–37

Oliveira PJ. 2009. Alternative derivation of differential constitutive equations of the Oldroyd-B type. *J. Non-Newton. Fluid Mech.* 160:40–46

Oliveira PJ. 2017. Reduced stress method for efficient computation of time-dependent viscoelastic flow with stress equations of FENE-P type. *J. Non-Newton. Fluid Mech.* 248:74–91

Oliveira PJ, Pinho FT, Pinto GA. 1998. Numerical simulation of non-linear elastic flows with a general collocated finite-volume method. *J. Non-Newton. Fluid Mech.* 79:1–43

Omowunmi SC, Yuan X-F. 2013. Time-dependent non-linear dynamics of polymer solutions in microfluidic contraction flow—a numerical study on the role of elongational viscosity. *Rheol. Acta* 52:337–54

Öttinger H-C, Laso M. 1992. Smart polymers in finite-volume calculations. In *Theoretical and Applied Rheology*, Vol. 1, ed. P Moldenaers, R Keunings, pp. 286–88. Amsterdam: Elsevier

Owens RG, Chauvière C, Philips TN. 2002. A locally-upwinded spectral technique (LUST) for viscoelastic flows. *J. Non-Newton. Fluid Mech.* 108:49–71

Owens RG, Phillips TN. 2002. *Computational Rheology*. London: Imp. Coll. Press

Palhares IL Jr., Oishi CM, Afonso AM, Alves MA, Pinho FT. 2016. Numerical study of the square-root conformation tensor formulation for confined and free-surface viscoelastic fluid flows. *Adv. Model. Simul. Eng. Sci.* 3:2

Park HM, Lim JY. 2010. A new numerical algorithm for viscoelastic fluid flows: the grid-by-grid inversion method. *J. Non-Newton. Fluid Mech.* 165:238–46

Perera MG, Walters K. 1977. Long-range memory effects in flows involving abrupt changes in geometry. *J. Non-Newton. Fluid Mech.* 2:49–81

Perot JB. 1993. An analysis of the fractional step method. *J. Comput. Phys.* 108:51–58
Phan-Thien N, Tanner RI. 1977. A new constitutive equation derived from network theory. *J. Non-Newton. Fluid Mech.* 2:353–65
Phillips TN, Williams AJ. 1999. Viscoelastic flow through a planar contraction using a semi-Lagrangian finite volume method. *J. Non-Newton. Fluid Mech.* 87:215–46
Pimenta F, Alves MA. 2016. *rheoTool*. OpenFOAM Toolbox, accessed April 30, 2020. **https://github.com/fppimenta/rheoTool**
Pimenta F, Alves MA. 2017. Stabilization of an open-source finite-volume solver for viscoelastic fluid flows. *J. Non-Newton. Fluid Mech.* 239:85–104
Pimenta F, Alves MA. 2019. A coupled finite-volume solver for numerical simulation of electrically-driven flows. *Comput. Fluids* 193:104279
Poole RJ, Alves MA, Oliveira PJ. 2007. Purely elastic flow asymmetries. *Phys. Rev. Lett.* 99:164503
Popinet S. 2020. *Basilisk*. Flow Solver, accessed Jan. 20. **http://basilisk.fr/**
Rajagopalan D, Armstrong RC, Brown RA. 1990. Finite element methods for calculation of steady, viscoelastic flow using constitutive equations with a Newtonian viscosity. *J. Non-Newton. Fluid Mech.* 36:159–92
Renardy M. 1985. Existence of slow steady flows of viscoelastic fluids with differential constitutive equations. *Z. Angew. Math. Mech.* 65:449–51
Renardy M. 1994. How to integrate the upper convected Maxwell (UCM) stresses near a singularity (and maybe elsewhere, too). *J. Non-Newton. Fluid Mech.* 52:91–95
Renardy M. 2000. Current issues in non-Newtonian flows: a mathematical perspective. *J. Non-Newton. Fluid Mech.* 90:243–59
Ribeiro VM, Coelho PM, Pinho FT, Alves MA. 2014. Viscoelastic fluid flow past a confined cylinder: three-dimensional effects and stability. *Chem. Eng. Sci.* 111:364–80
Richter D, Iaccarino G, Shaqfeh ESG. 2010. Simulations of three-dimensional viscoelastic flows past a circular cylinder at moderate Reynolds numbers. *J. Fluid Mech.* 651:415–42
Roache PJ. 1972. *Computational Fluid Dynamics*. Albuquerque, NM: Hermosa
Sahin M, Wilson HJ. 2007. A semi-staggered dilation-free finite volume method for the numerical solution of viscoelastic fluid flows on all-hexahedral elements. *J. Non-Newton. Fluid Mech.* 147:79–91
Saramito P. 2014. On a modified non-singular log-conformation formulation for Johnson-Segalman viscoelastic fluids. *J. Non-Newton. Fluid Mech.* 211:16–30
Saramito P, Wachs A. 2017. Progress in numerical simulation of yield stress fluid flows. *Rheol. Acta* 56: 211–30
Sasmal GP. 1995. A finite volume approach for calculation of viscoelastic flow through an abrupt axisymmetric contraction. *J. Non-Newton. Fluid Mech.* 56:15–47
Sato T, Richardson SM. 1994. Explicit numerical simulation of time-dependent viscoelastic flow problems by a finite element/finite volume method. *J. Non-Newton. Fluid Mech.* 51:249–75
Sommerfeld M. 2017. Numerical methods for dispersed multiphase flows. In *Particles in Flows. Advances in Mathematical Fluid Mechanics*, ed. T Bodnár, G Galdi, Š Nečasová, pp. 327–96. Cham, Switz.: Springer Int.
Sousa PC, Pinho FT, Alves MA. 2018. Purely-elastic flow instabilities and elastic turbulence in microfluidic cross-slot devices. *Soft Matter*. 14:1344–54
Sousa PC, Pinho FT, Oliveira MSN, Alves MA. 2015. Purely elastic flow instabilities in microscale cross-slot devices. *Soft Matter* 11:8856–62
Sousa RG, Poole RJ, Afonso AM, Pinho FT, Oliveira PJ, et al. 2016. Lid-driven cavity flow of viscoelastic liquids. *J. Non-Newton. Fluid Mech.* 234:129–38
Spanjaards MMA, Hulsen MA, Anderson PD. 2019. Transient 3D finite element method for predicting extrudate swell of domains containing sharp edges. *J. Non-Newton. Fluid Mech.* 270:79–95
Su J, Ouyang J, Wang X, Yang B, Zhou W. 2013. Lattice Boltzmann method for the simulation of viscoelastic fluid flows over a large range of Weissenberg numbers. *J. Non-Newton. Fluid Mech.* 194:42–59
Sun J, Phan-Thien N, Tanner RI. 1996. An adaptive viscoelastic stress splitting scheme and its applications: AVSS/SI and AVSS/SUPG. *J. Non-Newton. Fluid Mech.* 65:75–91
Sun J, Smith MD, Armstrong RC, Brown RA. 1999. Finite element method for viscoelastic flows based on the discrete adaptive viscoelastic stress splitting and the discontinuous Galerkin method: DAVSS-G/DG. *J. Non-Newton. Fluid Mech.* 86:281–307

Sureshkumar R, Beris AN. 1995. Effect of artificial stress diffusivity on the stability of numerical calculations and the flow dynamics of time-dependent viscoelastic flows. *J. Non-Newton. Fluid Mech.* 60:53–80
Sureshkumar R, Beris AN, Handler RA. 1997. Direct numerical simulation of the turbulent channel flow of a polymer solution. *Phys. Fluids* 9:743–55
Syrakos A, Dimakopoulos Y, Tsamopoulos J. 2020. A finite volume method for the simulation of elastoviscoplastic flows and its application to the lid-driven cavity case. *J. Non-Newton. Fluid Mech.* 275:104216
Tang D, Marchesini FH, Cardon L, D'hooge DR. 2019. Three-dimensional flow simulations for polymer extrudate swell out of slit dies from low to high aspect ratios. *Phys. Fluids* 31:93103
ten Bosch BIM. 1999. On an extension of dissipative particle dynamics for viscoelastic flow modelling. *J. Non-Newton. Fluid Mech.* 83:231–48
Thomases B. 2011. An analysis of the effect of stress diffusion on the dynamics of creeping viscoelastic flow. *J. Non-Newton. Fluid Mech.* 166:1221–28
Tomé MF, Araújo MSB, Alves MA, Pinho FT. 2008. Numerical simulation of viscoelastic flows using integral constitutive equations: a finite difference approach. *J. Comput. Phys.* 227:4207–43
Vaithianathan T, Collins LR. 2003. Numerical approach to simulating turbulent flow of a viscoelastic polymer solution. *J. Comput. Phys.* 187:1–21
Vaithianathan T, Robert A, Brasseur JG, Collins LR. 2006. An improved algorithm for simulating three-dimensional, viscoelastic turbulence. *J. Non-Newton. Fluid Mech.* 140:3–22
Vaithianathan T, Robert A, Brasseur JG, Collins LR. 2007. Polymer mixing in shear-driven turbulence. *J. Fluid Mech.* 585:487–97
Valente PC, da Silva CB, Pinho FT. 2014. The effect of viscoelasticity on the turbulent kinetic energy cascade. *J. Fluid Mech.* 760:39–62
van Os RGM, Phillips TN. 2004. Spectral element methods for transient viscoelastic flow problems. *J. Comput. Phys.* 201:286–314
Varchanis S, Hopkins CC, Shen AQ, Tsamopoulos J, Haward SJ. 2019a. Asymmetric flows of complex fluids past confined cylinders: a comprehensive numerical study with experimental validation. *Phys. Fluids* 32:053103
Varchanis S, Makrigiorgos G, Moschopoulos P, Dimakopoulos Y, Tsamopoulos J. 2019b. Modeling the rheology of thixotropic elasto-visco-plastic materials. *J. Rheol.* 63:609–39
Vázquez-Quesada A, Ellero M, Español P. 2012. An-SPH based particle model for computational microrheology. *Microfluid. Nanofluid.* 13:249–60
Verbeeten WMH, Peters GWM, Baaijens FPT. 2001. Differential constitutive equations for polymer melts: the extended Pom-Pom model. *J. Rheol.* 45:823–843. Erratum. 2001. *J. Rheol.* 45:1489
Walters K. 1982. Special issue on "Numerical simulation in non-Newtonian fluid mechanics." *J. Non-Newton. Fluid Mech.* 10:1
Waters ND, King MJ. 1970. Unsteady flow of an elastico-viscous liquid. *Rheol. Acta* 9:345–55
Xue SC, Phan-Thien N, Tanner RI. 1998. Three dimensional numerical simulations of viscoelastic flows through planar contractions, *J. Non-Newton. Fluid Mech.* 74:195–245
Xue SC, Tanner RI, Phan-Thien N. 2004. Numerical modelling of transient viscoelastic flows. *J. Non-Newton. Fluid Mech.* 123:33–58
Yoo JY, Na Y. 1991. A numerical study of the planar contraction flow of viscoelastic fluids using the SIMPLER algorithm. *J. Non-Newton. Fluid Mech.* 39:89–106
Zografos K, Burshtein N, Shen AQ, Haward SJ, Poole RJ. 2018. Elastic modifications of an inertial instability in a 3D cross-slot. *J. Non-Newton. Fluid Mech.* 262:12–24

RELATED RESOURCES

Astarita G, Marrucci G. 1974. *Principles of Non-Newtonian Fluid Mechanics*. Maidenhead, UK: McGraw-Hill
Beris AN, Edwards BJ. 1994. *Thermodynamics of Flowing Systems with Internal Microstructure*. New York: Oxford Univ. Press
Huilgol RR. 2015. *Fluid Mechanics of Viscoplasticity*. Berlin: Springer

Larson RG. 1999. *The Structure and Rheology of Complex Fluids*. New York: Oxford Univ. Press
Öttinger H-C. 1996. *Stochastic Processes in Polymeric Fluids: Tools and Examples for Developing Simulation Algorithms*. Berlin: Springer
Patankar SV. 1980. *Numerical Heat Transfer and Fluid Flow*. Washington, DC: Hemisphere
Versteeg HK, Malalasekera W. 2007. *An Introduction to Computational Fluid Dynamics: The Finite Volume Method*. New York: Prentice Hall. 2nd ed.

Annual Review of Fluid Mechanics

Volume 53, 2021

Contents

Indexes

Errata

An online log of corrections to *Annual Review of Fluid Mechanics* articles may be found at http://www.annualreviews.org/errata/fluid